Chapter - 4

Effect of L-Arginine on Structural, Thermal, Electrical and Optical Properties of Potassium Dihydrogen Phosphate (KDP)

Chapter-4: Effect of L-Arginine on Structural, Electrical and Optical Properties of Potassium Dihydrogen Phosphate (KDP) Crystals

1. Introduction:

Single crystal growth is significant in today's world of rapid technological and scientific progress, and the use of crystals presently has no limits. As a result, single crystal growth and its characterizations are most relevant for advancing material science research [1]. The two well-known non-linear materials, potassium dihydrogen phosphate (KDP) and ammonium dihydrogen phosphate (ADP), have appropriate structural qualities, high laser damage thresholds, massive non-linear optical coefficients, and robust mechanical properties [2]. Because of its electro-optic effect, KDP is commonly used to obtain phase and amplitude modulations. KDP's ability to produce higher-power second and third harmonics is one of the most promising materials for Nd: YAG and Nd: glass laser excitation. Non-linear optical (NLO) materials in single crystal form have been in high demand for rapid high-density data storage, data retrieval, and transmission. These single crystals have various applications, including high-energy lasers, initial confinement fusion study [3], electro-optic switches, colour light, frequency transfer, and so on [4]. Electro-optic phase modulators are used in signal processing devices to produce optical parametric frequency conversion, amplitude modulation, and switching.

There have been quite a large number of organic and inorganic materials synthesized for NLO applications; however, they have several drawbacks, including poor optical efficiency, low optical transmittance, low laser damage levels in some cases, and inability to be in large crystal forms. Due to the weak Van der Waals forces of hydrogen bonds, which bind them together, organic crystals have low mechanical properties. Because of their crystal structures, many NLO materials have a high anisotropic response to electromagnetic radiation. The reliability of non-linear performance can be improved by doping the NLO material appropriately when an organic material having a non-linear π-conjugate is mixed with an ionic salt, a new favourable NLO material; so-called semi-organic is formed. Besides being a distinctive ferroelectric material with hydrogen bonding, KDP is a widely used electro-optic, piezoelectric, and display application material. Recent findings indicate that such habit-modifying additives can be used to alter crystal morphology and growth rates. This can aid in the selection of the best crystal size and cut. However, controlling crystal habit and its modification, or the ratio of crystal dimensions along the crystallographic axes x, y, and z, is

quite challenging. Certain additives can be used to improve crystal morphology and alter growth rates; however, these additives must have the ability to bind to particular crystal planes. Filterability, handling, and compaction have also become essential aspects of industrial crystallization, as habit alteration often results in changes in the overall shape and size of the crystal [5].

NLO properties are found in amino acids with characteristics of concern, such as **(i)** zwitterionic nature, **(ii)** the molecular chirality and **(iii)** the lack of tightly conjugated bonds. When amino acid-based dopants are augmented with KDP, optical and other properties improve significantly. In this present study, we have doped KDP with L-Arginine. Electrical properties, optical properties, second harmonic generation efficiency and other properties of KDP have been observed to be modified with the doping of L-Arginine in several reported studies [6,7]. Amino acids also have significant hyperpolarizabilities in both donor and acceptor molecules [8,11]. Because of their low dielectric constants, amino acid doped salt materials are ideal for microelectronics. Ferroelectric materials fulfil this criterion. An additional advantage of amino acid doped KDP crystals is their ability to withstand repeated exposure to high power density laser radiation without inducing strain and subsequent inhomogeneities in the refractive index. We have grown pure KDP and L-Arginine (1 mol% and 2 mol%) doped KDP crystals using the slow evaporation solution method. Powder X-ray Diffraction (XRD) analysis, Dielectric Measurements, Fourier Transform Infrared spectroscopy (FTIR), Ultraviolet-Visible (UV-Visible) spectroscopy and relative Second Harmonic Generation (SHG) efficiency analysis were performed to study different changes in the grown crystals. The crystal growth using the slow evaporation technique and the effect of L-Arginine doping are presented and discussed in the following sections.

2. Experimental:

The slow evaporation technique was used to grow pure and L-Arginine (1 mol% and 2 mol%) doped KDP crystals. A detailed discussion of the evaporation method of the solution growth process has been given in chapter-3.

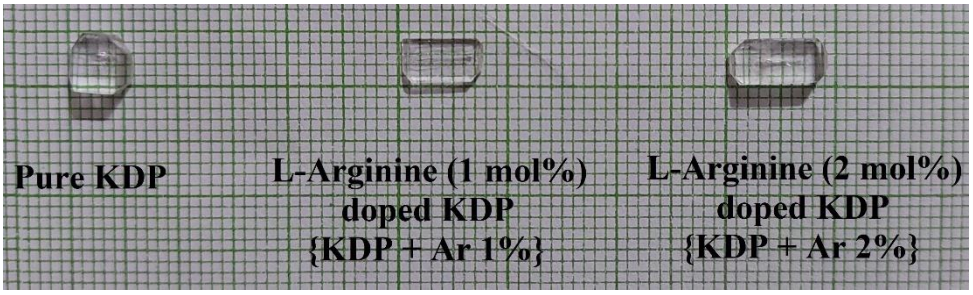

Figure 1. Grown crystals of pure KDP and L-Arginine doped KDP

3. Results and Discussion:

3.1 Powder X-Ray Diffraction (XRD) Analysis:

The XRD plots of pure KDP and L-Arginine (1 mol% and 2 mol%) doped KDP crystals are shown in figure 2(a). The powdered samples were scanned in 0.019° angular increments over a 2θ range of 10° to 80°. There is no phase shift in the crystal due to doping, as seen in the XRD plot. In addition, pure and doped KDP crystals have sharp prominent diffraction peaks, indicating excellent crystalline perfection [12]. The powder XRD patterns of pure KDP and L-Arginine doped KDP demonstrate that they belong to the tetragonal system with space group ($1\bar{4}2d$). The XRD peaks of doped crystals show that it is in a single phase. Figure 2(b) depicts the shifting of specific prominent peak resulting from the inclusion of the dopant. However, this shift is considered negligible. The shift could be due to tension on the lattice caused by amino acid absorption in the KDP lattice. Due to the addition of dopants, there is a slight change in lattice parameter values, and as a result, some of the significant peaks are observed to be shifted. FullProf suite software was used to index and analyze XRD patterns, and the derived cell parameters are listed in table 1. Also, there are small deviations in calculated values of lattice parameters of doped crystals from pure KDP crystal. These results suggest that the presence of dopants do not affect the crystal's basic structure. In addition, the relative intensity of peaks was found to vary in doped KDP crystals. This is a sign of a change in molecular conformation due to doping, no matter how slight it is. Table 2 depicts the change in structural parameters of pure KDP and doped KDP crystals.

Table 1. Lattice parameters of pure & L-Arginine doped KDP crystals

Crystals	a (Å)	b (Å)	c (Å)	Volume	Symmetry
Pure KDP (Reported)	7.448	7.448	6.977	387.033	Tetragonal
Pure KDP	7.453	7.453	6.975	387.456	
KDP + Ar 1%	7.449	7.449	6.975	387.062	
KDP + Ar 2%	7.452	7.452	6.974	387.414	

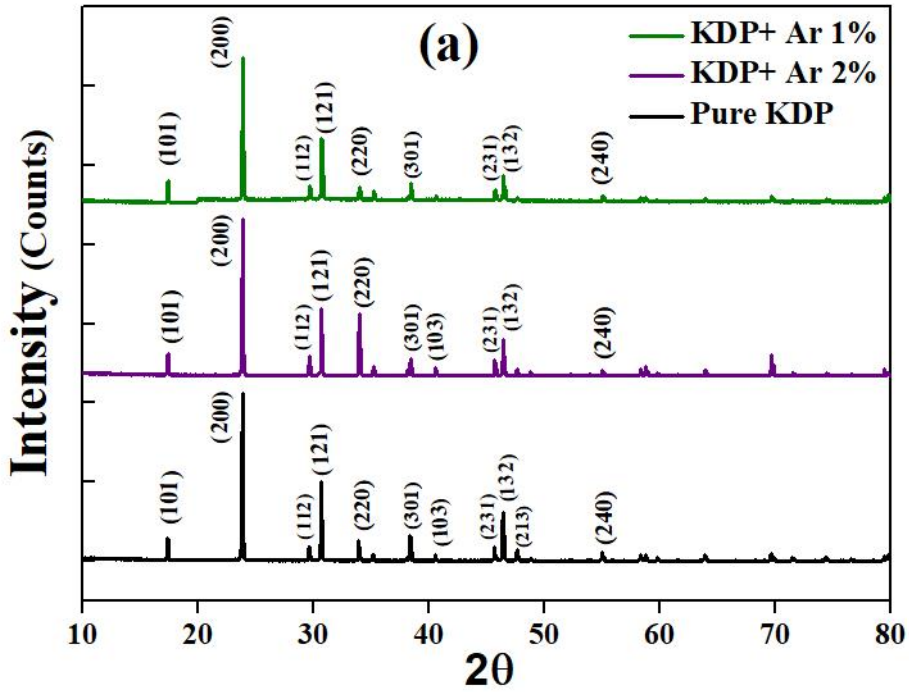

Figure 2(a). Powder XRD plots of pure and L-Arginine doped KDP crystals

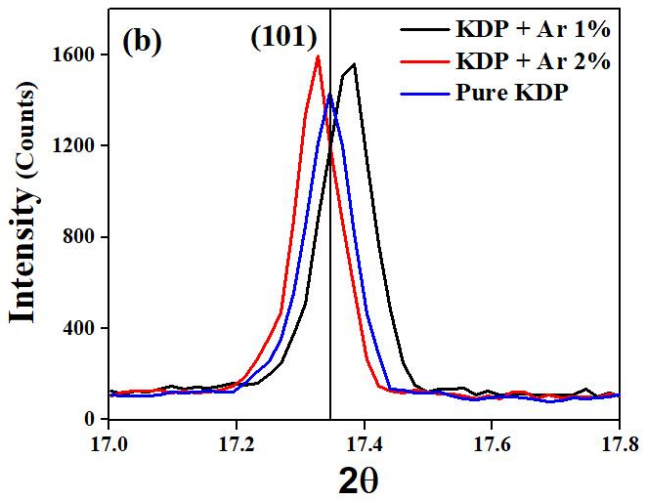

Figure 2(b). Peak (101) shifting of pure, and L-Arginine doped KDP crystals

Table 2. Structural parameters of pure and doped KDP crystals

Sample	FWHM	2θ	Crystallite Size t (nm)	Strain ε ($lin^{-2} m^{-4}$)	Dislocation Density δ ($lin\ m^{-4}$)
Pure KDP	0.09	17.34	1.55	2.22E-02	2.87E-02
	0.1182	23.81	1.19	2.89E-02	4.86E-02
	0.0822	30.64	1.74	1.98E-02	2.29E-02
KDP + Ar 1%	0.0958	17.37	1.46	2.37E-02	3.26E-02
	0.0953	23.83	1.48	2.33E-02	3.16E-02
	0.0666	30.66	2.15	1.61E-02	1.50E-02
KDP + Ar 2%	0.0857	17.32	1.63	2.12E-02	2.61E-02
	0.1093	23.85	1.29	2.67E-02	4.15E-02
	0.1565	30.71	0.91	3.77E-02	8.27E-02

3.2 Dielectric Analysis:

Dielectric investigations of pure KDP and L-Arginine doped KDP crystals were conducted in the frequency range of 100 Hz to 100 kHz and in the temperature range of 323 K - 373 K. Z-view software was used to evaluate the data obtained. Impedance spectroscopy is a prominent analytical tool in materials research and development because its results may correlate to ion transfer mechanisms, dielectric characteristics, defects, conductance in solids, etc. Furthermore, the material's dielectric characteristics provide a significant tool for studying the lattice dynamics of a crystal. On the other hand, complex modulus spectroscopy is more advantageous in studying electronic transport in crystals. The movement of hydrogen within a framework and defects such as proton migration and additional hydrogen bonds cause protonic conduction in KDP. The complex impedance spectroscopy, conduction mechanism, modulus spectroscopy and dielectric spectroscopy of pure and varied weight percentage L-Arginine doped KDP crystals as a function of frequency and temperature are investigated and presented in this section. The dielectric constant and dielectric loss were calculated using the formulae,

$$\varepsilon' = \frac{-Z''}{\omega C_o\left(Z'^2+Z''^2\right)} \quad (1)$$

$$\varepsilon'' = \frac{Z'}{\omega C_o\left(Z'^2+Z''^2\right)} \quad (2)$$

where, Z' is the real part of the complex impedance and is given as $Z' = |Z| \cos\theta$ and Z'' is the imaginary part of the complex impedance and is given as $Z'' = |Z| \sin\theta$.

The variation of the dielectric constant with an angular frequency of the applied field at different temperatures for pure and various L-Arginine doped KDP crystals is shown in figures

3(a-b). At low frequencies, the value of the dielectric constant is high, and it decreases as frequency increases. Various polarization mechanisms, namely, electronic, ionic, orientational and space charge polarization, explain the high dielectric constant at lower frequencies [13]. The sudden plummeting nature of the dielectric constant at high frequency is due to dipoles that cannot comply with applied a. c electric field variations. Moreover, as the temperature rises, the dielectric constant increases in the lower frequency region as more dipoles orient themselves along the field, resulting in an increased value of dipole moment [14,15].

Due to the discharge of space charge, the dielectric constants of all crystals converge at higher frequencies. The magnitude of the dielectric constant of 2 mol% L-Arginine doped KDP crystal is more significant than that of 1 mol% L-Arginine doped KDP and pure KDP crystal, as shown in figures 3(a-b). The behaviour of the highest dielectric constant of 2 mol% L-Arginine doped KDP crystal may be explained based on interfacial polarization with Koop's phenomenological theory or Maxwell-Wagner two layers model [16,17]. This model states that the dielectric materials are usually composed of many well-conducting grains separated by poorly conducting thin grain boundaries. Charge carriers can quickly move from the grain interior and congregate at grain boundaries when an external electric field is applied, leading to large polarization and a high dielectric constant value.

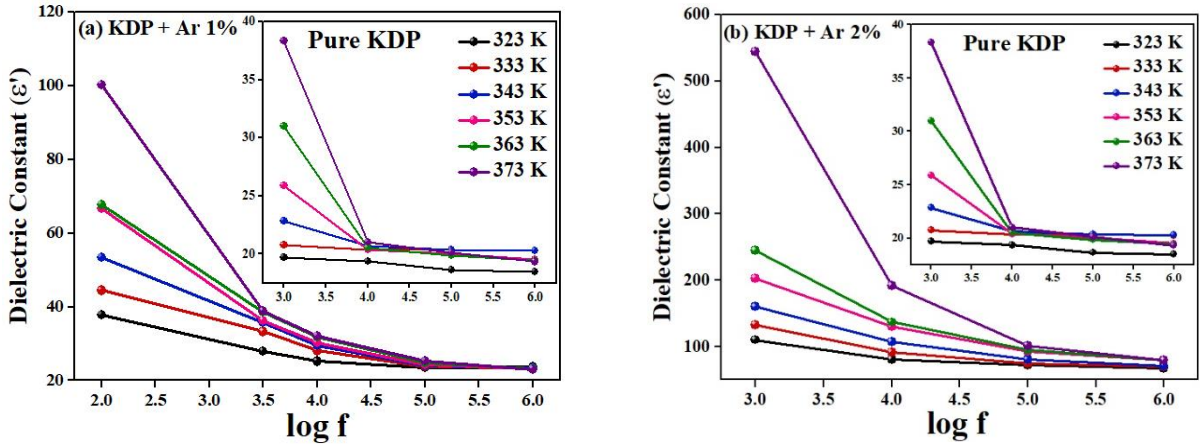

Figures 3. (a) The dielectric constant of pure KDP and L-Arginine (1 mol%) doped KDP crystals and **(b)** The dielectric constant of pure KDP and L-Arginine (2 mol%) doped KDP crystals

Figures 3(c-d) show how dielectric loss varies with applied field angular frequency at various temperatures for pure and L-Arginine (1 mol% and 2 mol%) doped KDP crystals. The same behaviour as the dielectric constant with frequency and temperature is observed with the dielectric loss for all crystals. Therefore, the lattice charge defect of the space charge polarization could explain the considerable value of the dielectric loss at low frequencies.

Moreover, when comparing the magnitudes of the dielectric losses of pure and L-Arginine doped KDP crystals, it is observed that pure KDP crystals have a high value of dielectric loss than doped KDP crystals. Hence, we can say that pure KDP crystal experiences more energy loss in terms of heat than in L-Arginine doped KDP crystals.

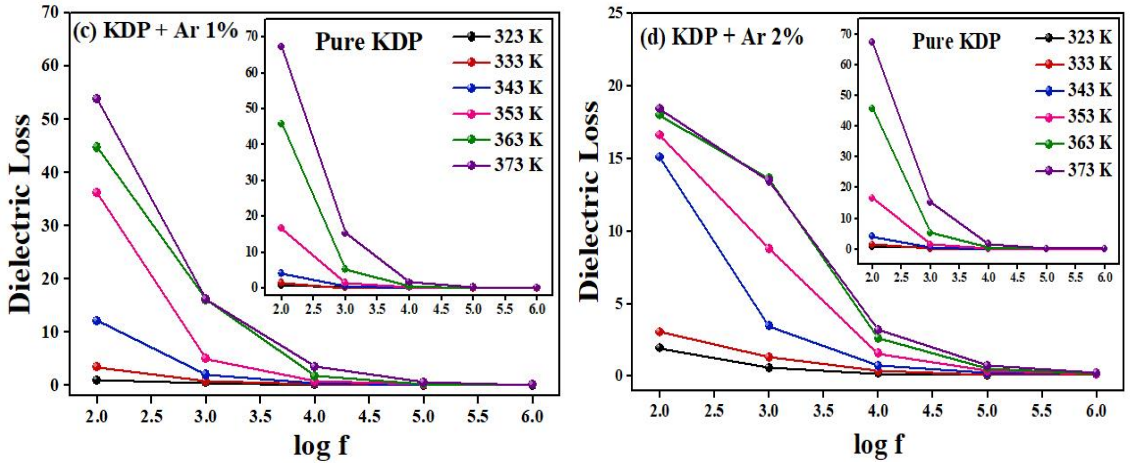

Figures 3. (c) The dielectric loss of pure and L-Arginine (1 mol%) doped KDP crystal and **(d)** The dielectric loss of pure and L-Arginine (2 mol%) doped KDP crystal

Additionally, the electro-optic coefficient (r_{eff}) of material is proportional to its dielectric constant. Therefore, the doped KDP crystals with a large dielectric constant might be employed to make more efficient electro-optic modulators [18]. While others having low dielectric constant can find an interlayer dielectric application in the microelectronic industry [19].

3.2.1 Impedance Spectroscopy:

Nyquist plots [real part of complex impedance (Z') versus imaginary part of complex impedance (Z'')] of pure and L-Arginine doped KDP crystals are shown in figures 4(a-c). Z-view software was used to examine the impedance results. For each temperature, a single semi-circular arc is seen. Due to temperature-dependent relaxation processes, the centre of each semicircle is below the axis. This means that all crystals (pure and doped) indicate non-Debye behaviour. A tail or spike is observed at lower frequencies because of the polarization of electrodes/electrolytes [20-22].

The magnitude of the real part of complex impedance (Z') for all crystals decreases as frequency and temperature increase, indicating an increase in a. c conductivity, as seen in figures 5(a-c). Additionally, when the frequency increases, the Z' at all temperatures merges and becomes constant for all crystals, possibly due to the discharge of space charges [23]. The

variation of the imaginary part of complex impedance (Z'') with respect to applied frequency and temperature for pure KDP and L-Arginine doped KDP crystals is shown in figures 6(a-c).

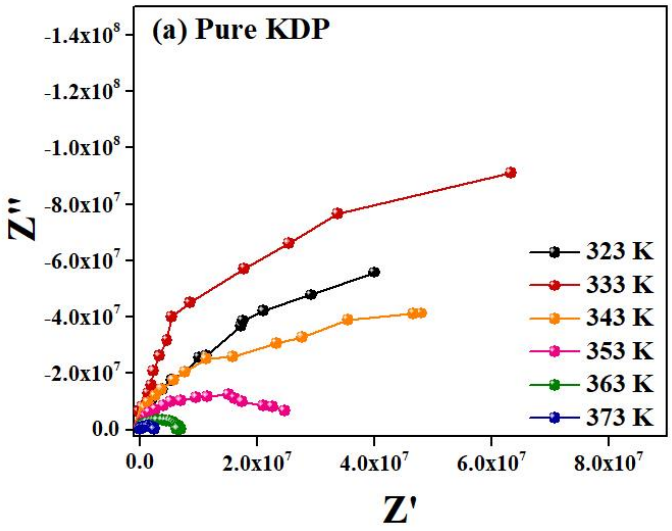

Figure 4(a). Nyquist plot of pure KDP crystal

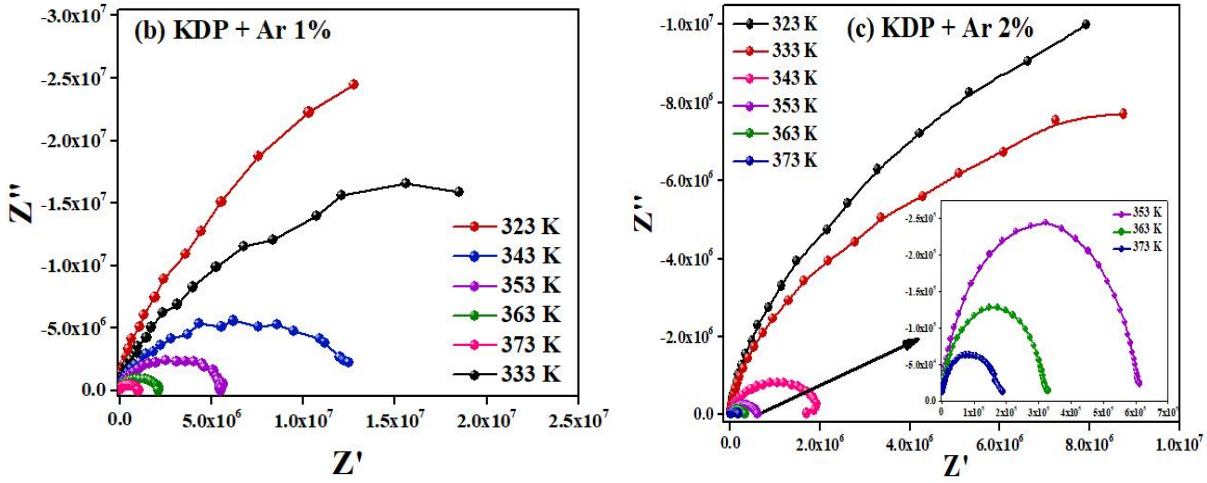

Figures 4. (b) Nyquist plot of L-Arginine (1 mol%) doped KDP crystal and **(c)** Nyquist plot of L-Arginine (2 mol%) doped KDP crystal

In each plot, there is only one peak. As the temperature rises, the maximum peak value lowers, the peak itself broadens and simultaneously, the peak maximum moves to higher frequency values. These results indicate that the crystal exhibits relaxation phenomena. The shifting of relaxation peaks indicates an increase in the rate of charge carrier hopping [24]. The relaxation time (τ) is the amount of time it takes for a charge carrier to recuperate from an external electric field perturbation. By fitting the semicircles of the Nyquist plot, the values of

grain boundary resistance, relaxation time capacitance is presented in table 3. The following equation [25] was used to calculate the relaxation time τ:

$$\tau = \frac{1}{2\pi f_{max}} \tag{3}$$

where, f_{max} is the frequency at Z''_{max}

The value of capacitance was calculated using the formula,

$$\omega_{max} RC = 1 \tag{4}$$

where, R is the bulk resistance or grain resistance obtained from the Nyquist plot and C is capacitance.

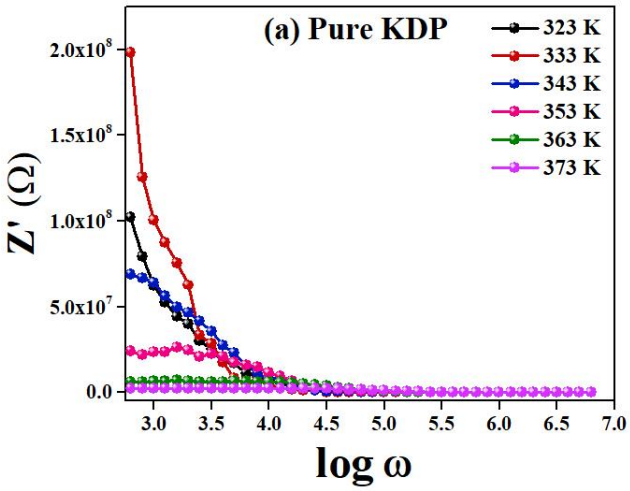

Figure 5(a). Z' versus log ω of pure KDP crystal

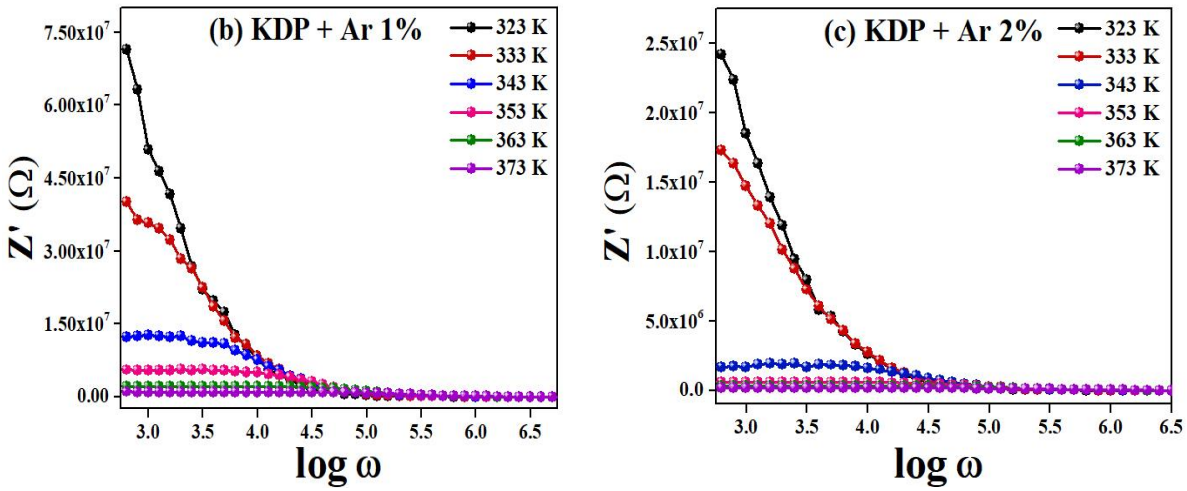

Figures 5. (b) Z' versus log ω of L-Arginine (1 mol%) doped KDP crystal and **(c)** Z' versus log ω of L-Arginine (2 mol%) doped KDP crystal

Table 3. Nyquist parameters of pure and L-Arginine doped KDP crystals

Temperature	KDP			KDP + Ar 1%			KDP + Ar 2%		
	R_g (Ω)	C_g (10^{-10}) F	τ (ms)	R_g (Ω)	C_g (10^{-10}) F	τ (ms)	R_g (Ω)	C_g (10^{-10}) F	τ (ms)
323 K	1.17E+09	2.957	1.2642	8.78E+07	38.099	1.0041	2.49E+07	134.052	1.0041
333 K	3.36E+08	9.629	0.7976	3.51E+07	81.700	0.3175	7.44E+06	421.100	0.6336
343 K	7.65E+07	40.961	0.6336	1.25E+07	196.384	0.0797	2.07E+06	1101.234	0.0399
353 K	2.61E+07	98.106	0.1264	5.77E+06	395.119	0.0399	6.08E+05	3432.333	0.0159
363 K	7.06E+06	339.060	0.0633	2.20E+06	929.118	0.0126	3.26E+05	6021.320	0.0079
373 K	2.50E+06	931.990	0.0503	1.01E+06	2028.759	0.0126	1.56E+05	12597.861	0.0079

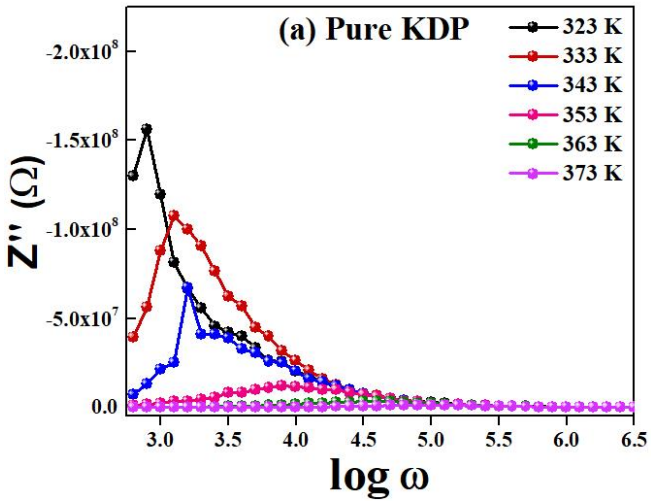

Figure 6(a). Variation in the imaginary part of impedance (Z′′) with frequency (f) for pure KDP crystal

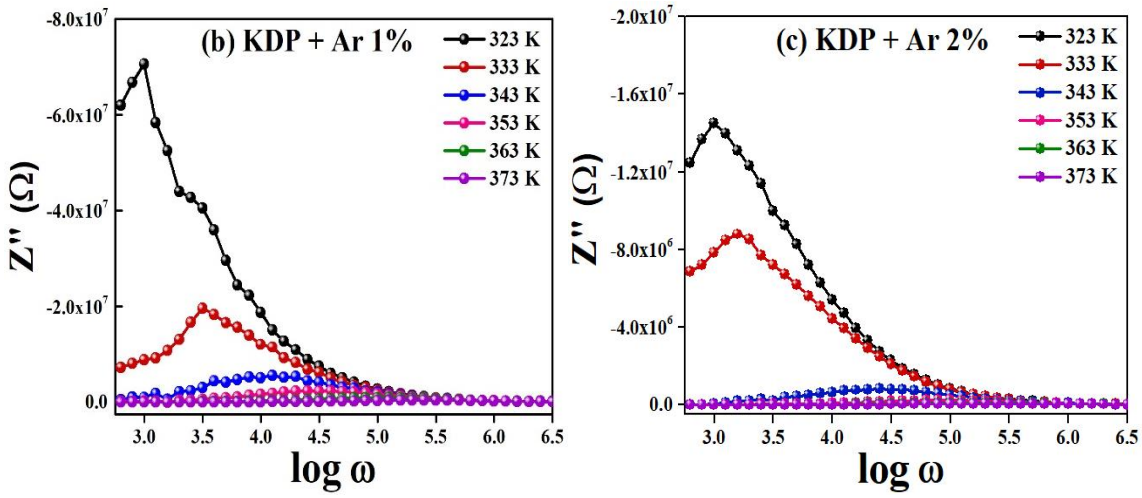

Figures 6. (b) Variation in the imaginary part of impedance (Z'') with frequency (f) for L-Arginine (1 mol%) doped KDP crystal and **(c)** Variation in the imaginary part of impedance (Z'') with frequency (f) for L-Arginine (2 mol%) doped KDP crystal

3.2.2 A. C Conductivity Mechanism:

The crystal's A. C conduction has been studied at temperatures ranging from 323 K to 373 K and frequencies ranging from 100 Hz to 1 MHz. A. C conductivity analysis provides comprehensive information on the time-dependent movement of charges resulting in conductivity and dielectric relaxation. It also offers helpful information on the electric field distribution in the system and field-induced perturbations [26]. Complex A. C conductivity can be written as,

$$\sigma^*(\omega) = \sigma'_{ac}(\omega) + \sigma''_{ac}(\omega) \quad (5)$$

where, $\sigma'_{ac}(\omega)$ is the real part and $\sigma''_{ac}(\omega)$ is the imaginary part of complex A. C conductivity, respectively.

However, the real part of the complex A. C conductivity $\{\sigma'_{ac}(\omega)\}$ is given as [27],

$$\sigma'_{ac}(\omega) = \left(\frac{Z'}{Z'^2 + Z''^2}\right)\frac{t}{A} \quad (6)$$

where, A is the cross-sectional area of the crystal used, t is the thickness, Z' is the real part and Z'' is the imaginary part of the complex impedance.

The a. c conductivity variation with the angular frequency of applied field at different temperatures for pure and various L-Arginine doped KDP crystals is shown in figures 7 (a-c). Due to the polarisation of the electrode and crystal interface, the conductivity value is lower at lower frequencies; however, it increases at higher frequencies and exhibits a highly dispersive behaviour, as seen in the figures. The increase in a. c conductivity with frequency and temperature could be due to trapped bound charge carriers in the crystal.

KDP behaves like an ionic conductor, the a. c conductivity behaviour with respect to frequency can be explained with the help of the Jump Relaxation Model (JRM), introduced by Funke [28]. According to this approach, conductivity in the low frequency range is due to ions' successful forward and backward hopping within localized regions. In contrast, the rate of successful hopping of ions may decrease beyond the low frequency range. Thus, dispersive conductivity is caused by a shift in the ratio of successful to unsuccessful hops.

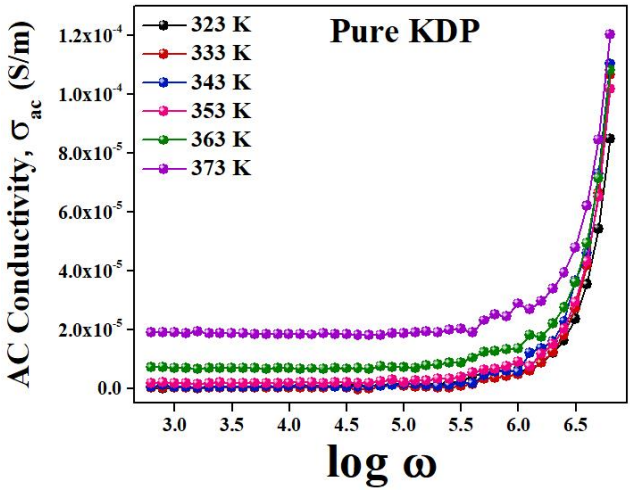

Figure 7(a). A. C Conductivity of pure KDP crystal

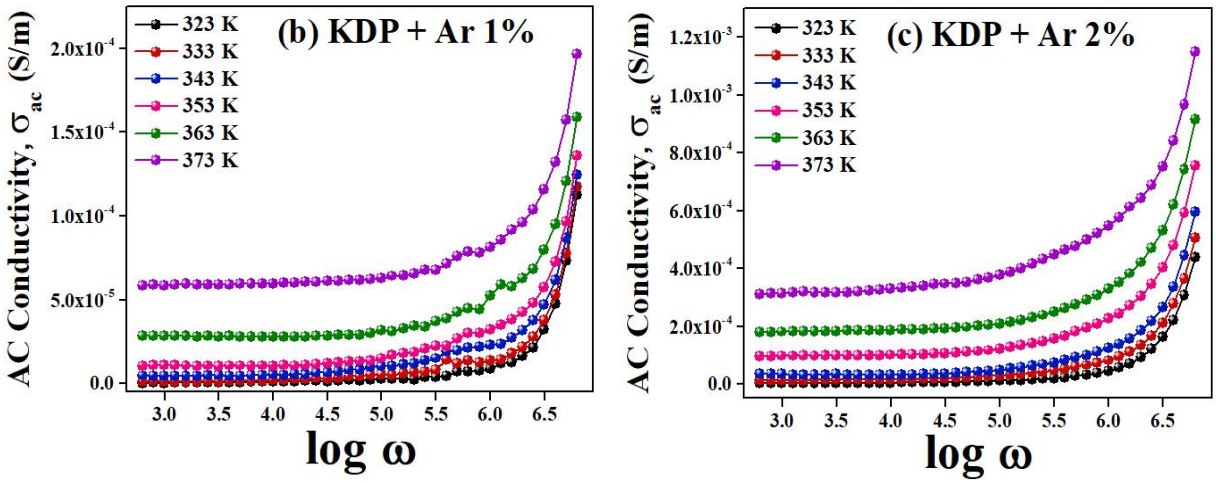

Figures 7. (b) A. C Conductivity of L-Arginine (1 mol%) doped KDP crystal and **(c)** A. C Conductivity of L-Arginine (2 mol%) doped KDP crystal

From the figures, the a. c conductivity of pure and L-Arginine doped KDP crystals rises linearly with temperature, indicating a thermally activated electrical conduction process within the crystal. When comparing the magnitudes of a. c conductivity of pure and doped crystals, implies that doping L-Arginine in KDP crystal increases the a. c conductivity, with the highest conductivity observed in L-Arginine (2 mol%) doped KDP crystal as compared to the conductivity of pure KDP crystal and L-Arginine (1 mol%) doped KDP crystal.

In general, KDP electric conductivity is ionic, wherein proton migration from localized sites has been observed. Within a KDP crystal molecule, two types of proton jumps are observed, intrabond and interbond, resulting in a vacancy (L-defect) and a doubly occupied bond (D-defect), respectively. These defects are responsible for conduction in KDP. L-Arginine molecules may occupy the interstitial position in the KDP crystal lattice up to a certain

amount of doping. In this circumstance, a hydrogen network of KDP molecules in a crystal might yield a significant number of hydrogen vacancies. Because conduction in KDP is protonic and primarily due to anions [$(H_2PO^4)^-$] rather than cations [$(NH_4)^+$], more hydrogen vacancies are produced, increasing the L-defect. This could be the reason for the higher a. c conductivity value in doped crystals compared to that of the pure KDP crystal. When the L-Arginine molecule is doped into the KDP crystal, the L-Arginine molecule will occupy the interstitial place due to its bigger size. Because it is a proton donor, it will donate hydrogen to KDP and subsequently combine with the KDP unit cell. However, due to low doping concentration, this occurs with relatively minor lattice distortion. When L-Arginine donates a proton to KDP, repulsion occurs between two protons that are each one from KDP and L-Arginine, due to which the hydrogen of KDP is removed as the bond between NH^{4+} and PO_4^{3-} is broken, and a hydrogen vacancy (L-defect) is formed. During this process, L-Arginine will join with KDP crystal at its defect sites. As a result, defects created by L-Arginine doping in KDP crystal may become a reason for the change in specific properties.

3.2.3 Jonscher's Plots:

The Jonscher power law (JPL) can be used to characterize most disordered materials at frequencies less than 10 MHz and temperatures more than 150 K [29]:

$$\sigma'_{ac}(\omega) = \sigma_0 + A\omega^s \quad (7)$$

where, $\omega = 2\pi f$ is the angular frequency of the applied voltage, σ_0 = d. c conductivity, A is a constant, s is a material property having a value between 0 to 1 [29].

Figures 8 (a-c) show Jonscher plots for pure and L-Arginine doped KDP crystals, which depicts highly dispersive behaviour due to the presence of a. c conductivity only. The slopes and intercepts of the plots in figure 7 were used to compute the values of s and A, listed in tables 4 and 5. If $s \leq 1$ in Jonscher's equation, it indicates sudden hopping motion caused by translational motion [28]. In ionic conductors, the value of 's' can typically vary from 1 to 0.5, indicating appropriate long-range routes and diffusion-limited hopping. By fitting equation (7), the value of exponent 's' and σ_0 are obtained at all temperatures. From table 4, it is observed that the value of d. c conductivity increases with the increase in dopant concentration as well as with increasing temperature. It is observed in table 5 that the 's' parameter value decreases linearly with temperature for pure, L-Arginine (1 mol% and 2 mol%) doped KDP crystals, implying a Correlation Barrier Hopping (CBH) conduction mechanism [30].

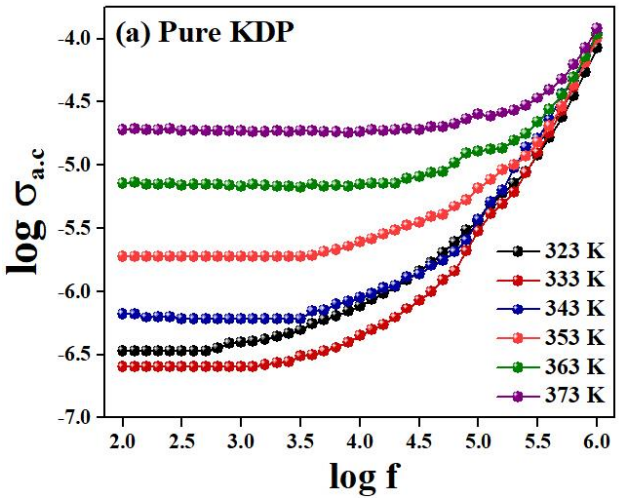

Figure 8(a). Jonscher's plot of pure KDP crystal

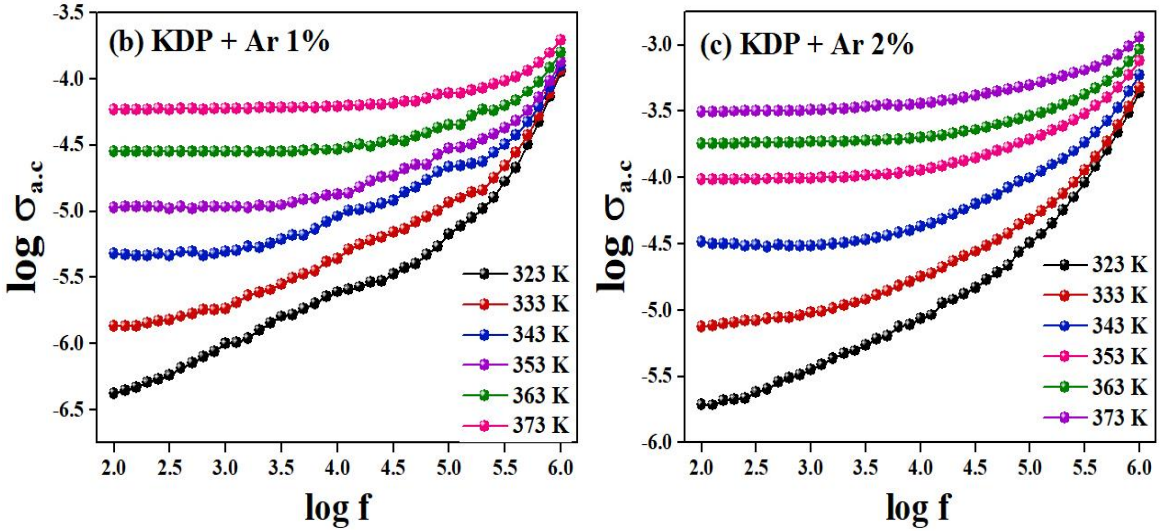

Figures 8. (b) Jonscher's plot of L-Arginine (1 mol%) doped KDP crystal and **(c)** Jonscher's plot of L-Arginine (2 mol%) doped KDP crystal

Table 4. $\sigma_{d.c}$ conductivity values of pure and L-Arginine (1 mol% and 2 mol%) doped KDP crystals

Temperature K	$\sigma_{d.c}$ conductivity		
	Pure KDP	KDP + Ar 1%	KDP + Ar 2%
323	0.8901×10^{-7}	3.98×10^{-7}	1.553×10^{-6}
333	0.92×10^{-7}	1.256×10^{-6}	7.0×10^{-6}
343	5.854×10^{-7}	4.536×10^{-6}	2.8586×10^{-5}
353	1.8236×10^{-6}	1.015×10^{-5}	0.9725×10^{-4}
363	0.7×10^{-5}	2.8075×10^{-5}	1.783×10^{-4}
373	1.885×10^{-5}	5.8×10^{-5}	3.1053×10^{-4}

Table 5. Jonscher's plot parameters for pure and L-Arginine (1 mol% and 2 mol%) doped KDP crystal

Temperature K	A			s - parameter		
	Pure KDP	KDP + Ar 1%	KDP + Ar 2%	Pure KDP	KDP + Ar 1%	KDP + Ar 2%
323	0.325E-08	0.4012E-08	1.663E-08	0.6252	0.6472	0.6556
333	0.3369E-08	0.8145E-08	2.56E-08	0.6021	0.6315	0.6456
343	0.3519E-08	1.25E-08	4.256E-08	0.5821	0.6215	0.6402
353	0.4021E-08	1.43E-08	4.863E-08	0.5624	0.6198	0.6324
363	0.5023E-08	1.725E-08	6.125E-08	0.5325	0.5925	0.6283
373	0.543E-08	1.985E-08	1.384E-07	0.5089	0.5842	0.6205

In this model, carriers conduct through barriers that separate the localized sites. In this model, the charge carriers are assumed to hop between defect centres over the potential barrier W_m that separates them. The separation R of the defect states is associated with the barrier height. The CBH model predicts that when the temperature rises, the value of 's' decreases and its value is given by,

$$s = 1 - \frac{6\,k_\beta T}{[W_m - k_B T\, ln(1/\tau_o)]} \tag{8}$$

where, τ_o is the characteristic relaxation time of the carriers, = 10^{-12} s, k_B is Boltzmann constant, T is the temperature and W_m is the binding energy, defined as the amount of energy required to completely remove an electron from one site and transfer it to another.

For a small value of T, $W_m \gg k_B T\, ln(1/\tau_o)$ and then equation (8) becomes [31],

$$s = 1 - \frac{6k_B T}{W_m} \tag{9}$$

From the slope of the linear plot of 1-s versus T, the binding energy W_m was calculated. The variation of 1-s with temperature for pure and L-Arginine doped KDP crystals is shown in figure 9. The slopes of the above mentioned linearly fitted plots are used to calculate the binding energies of all crystals for the CBH conduction mechanism.

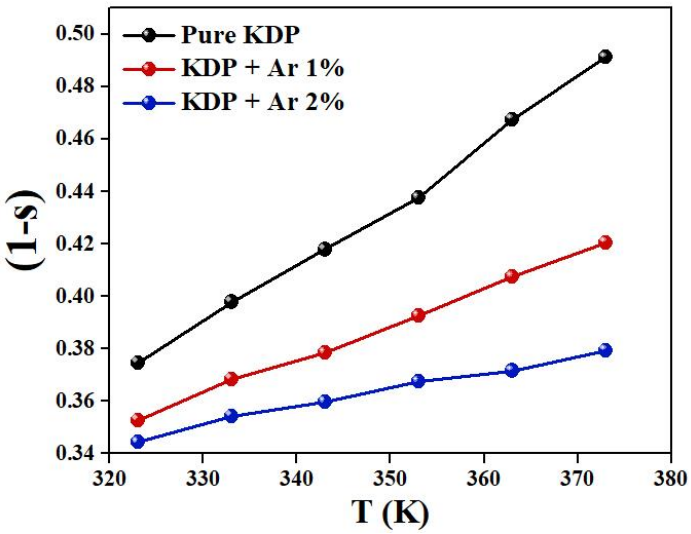

Figure 9. Binding energy plot of pure and L-Arginine (1 mol % and 2 mol%) doped KDP crystals

The value of binding energy for pure KDP crystal is 0.2238 eV, for L-Arginine (1 mol%) doped KDP crystal, it is 0.3858 eV, and for L-Arginine (2 mol%) doped KDP crystal, it is 0.7693 eV. The a. c conductivity was calculated using the CBH model [32]:

$$\sigma_{ac} = \frac{\pi^2}{12} . e^2 k_B T \omega \alpha^{-5} \left[N(E_f)\right]^2 \left[ln \frac{f_o}{\omega}\right]^4 \quad (10)$$

where, e is the electron charge, $\left[N(E_f)\right]$ is the density of states at the Fermi level, f_o is the photon frequency (=10^{13} Hz), $\alpha^{-1} = 10^{10}\ m^{-1}$ is localized wave and ω is the angular frequency.

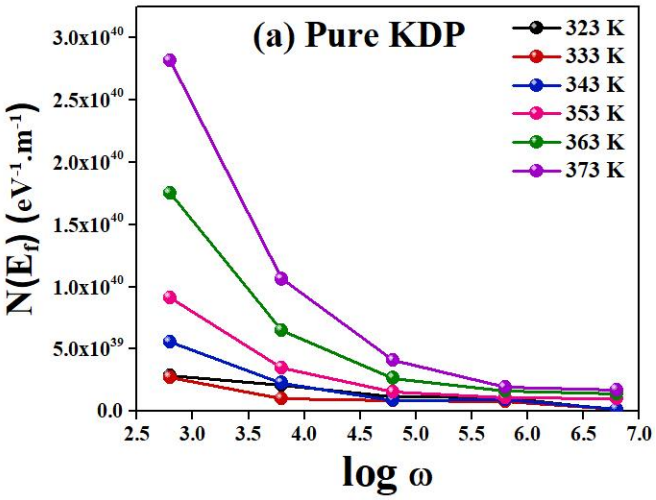

Figure 10(a). Density of states at Fermi level of pure KDP

The density of states at the Fermi level $[N(E_f)]$ is obtained by graphing the above equation over the angular frequency range. The variation of density of states at Fermi level, $[N(E_f)]$ versus angular frequency for pure and L-Arginine doped KDP crystals is shown in figures 10 (a-c). With increasing frequency, the density of states $[N(E_f)]$ of pure KDP and L-Arginine doped KDP crystals decreases.

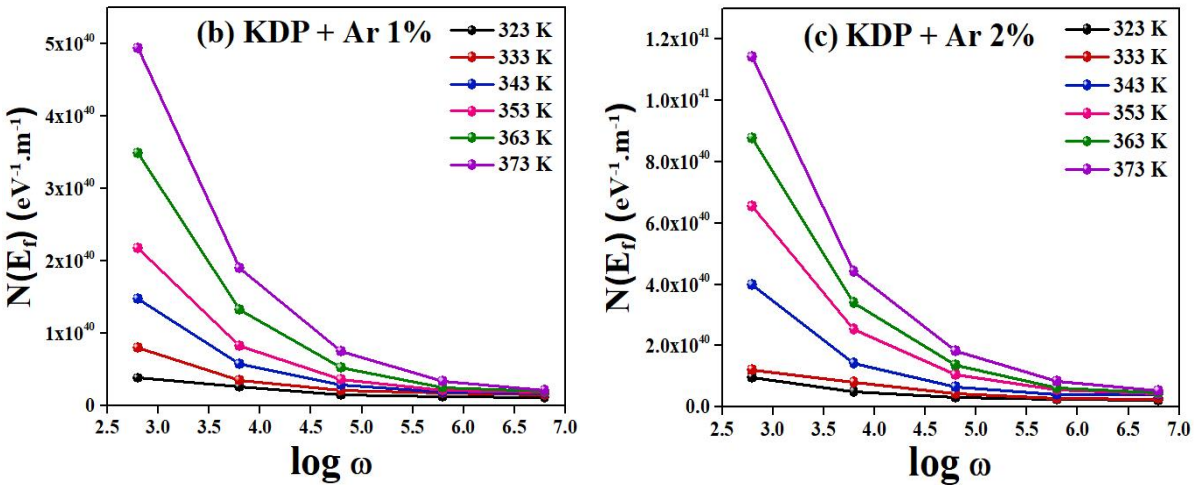

Figures 10. (b) Density of states at Fermi level of L-Arginine (1 mol%) doped KDP crystal and **(c)** Density of states at Fermi level of L-Arginine (2 mol%) doped KDP crystal

However, it is observed that at low frequencies, the value of $[N(E_f)]$ is seen to increase as the temperature rises. The relatively large values $[N(E_f)]$ of show that charge transport is dominated by hopping between pairs of sites. The barrier height for charge carrier hopping between different localized sites will be reduced due to this increase, allowing them to bounce between these localized sites more easily [33]. The high density of states at the Fermi level in the region of 10^{39}-10^{41} $(eV.m)^{-1}$ indicates that the CBH conduction mechanism is extremely suited for these respective materials and the temperature zone studied.

Figures 11(a-c) demonstrate the variation of $\log_{a.c}$ versus 1000/T for pure and L-Arginine doped KDP crystals at different frequencies. It can be observed that with the CBH conduction mechanism, the conductivity decreases as the reciprocal of temperature increases. Such behaviour indicates that conductivity is a thermally induced process for various localized states in many materials [34]. The Arrhenius type behaviour of a. c conductivity is suggested by the linear fitting of such curves as given by,

$$\sigma = \sigma_o . exp\left(\frac{E_a}{k_B T}\right) \quad (11)$$

where, σ is the a. c conductivity, E_a is the activation energy, σ_o is the pre-exponential factor, T is the temperature and k_B is the Boltzmann constant.

The activation energies of pure and L-Arginine doped KDP crystals were estimated from the slopes of linear fitted curves of log $\sigma_{a.c}$ versus 1000/T. Table 6 summarises the results obtained.

Table 6. Activation energies of pure and L-Arginine doped KDP crystals

Frequency	Activation Energy (E_a) (eV)		
	Pure KDP	KDP + Ar 1%	KDP + Ar 2%
100	1.2382	1.0444	1.0302
1000	1.1775	0.8444	1.0188
10000	1.1300	0.6676	0.8099
100000	0.7133	0.4504	0.5724
1000000	0.0310	0.1118	0.1943

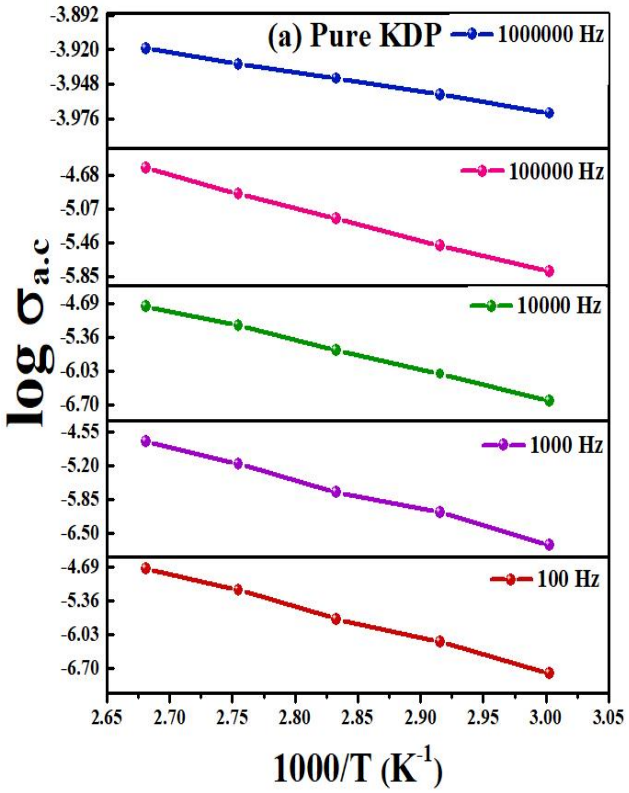

Figure 11(a). Activation energies plot for pure KDP crystal

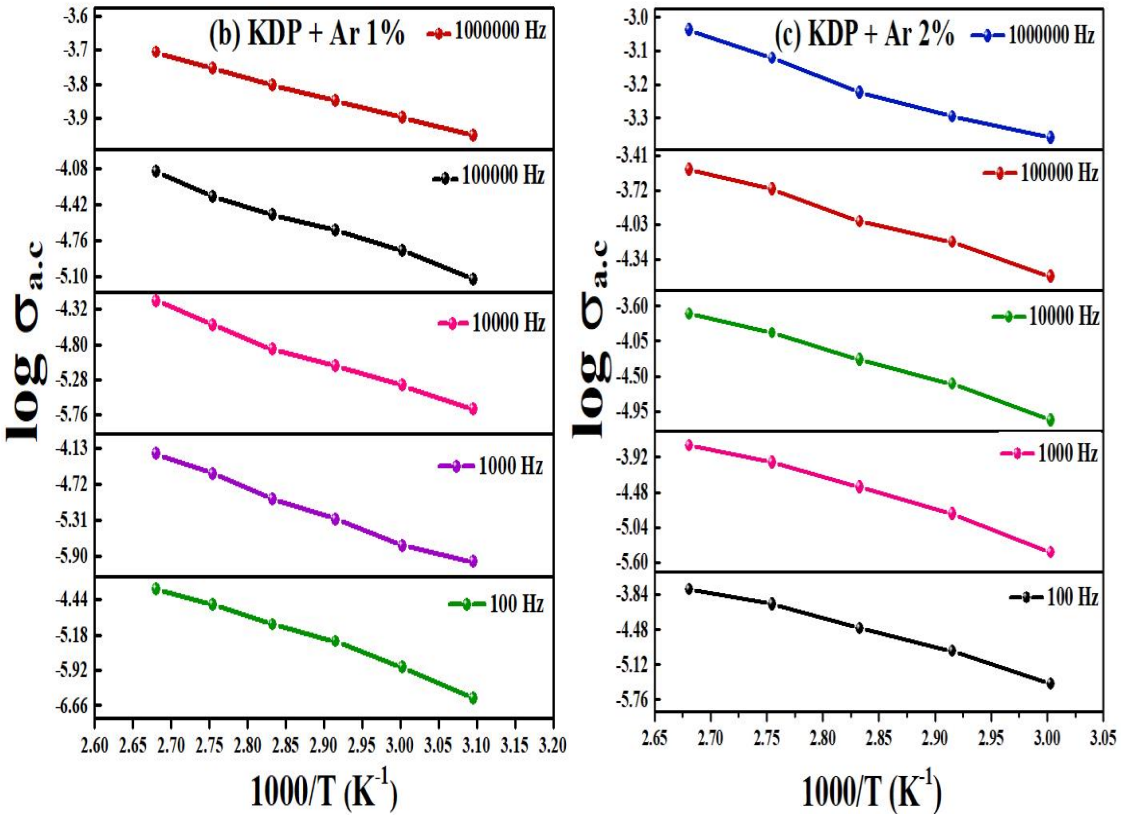

Figures 11. (b) Activation energies plot for L-Arginine (1 mol%) doped KDP crystal and **(c)** Activation energies plot for L-Arginine (2 mol%) doped KDP crystal

Table 4 shows that the activation energies for pure KDP and L-Arginine (1 mol% and 2 mol%) doped KDP crystals decrease as the frequency increases, implying that the electronic charge carriers easily jump across different localized states in the material [35].

3.2.4 Complex Modulus Spectroscopy:

Modulus analysis is a distinct way to investigate the electrical characteristics and enhance any other effects that may be present in the sample due to variable relaxation time constants. Figures 12 (a-c) shows the complex modulus plane plots in the temperature range 323 K - 373 K. The following formulae determine the values of the real and imaginary components of the modulus:

$$M' = \omega C_o Z'' \tag{12}$$

$$M'' = \omega C_o Z' \tag{13}$$

where, $C_o = \frac{\varepsilon_o A}{d}$ is the capacitance of parallel plate capacitor with air as a dielectric medium, A is the area of electrodes/plate used, and d is the crystal's thickness.

The complex modulus plots of pure and L-Arginine (1 mol% and 2 mol%) doped KDP crystals at various temperatures are shown in figures 12 (a-c). All crystals whose centres do not lie on the real axis exhibit one semicircle, suggesting non-Debye type relaxation inside crystals. Here, the first semicircle at lower frequency comprises of grain contribution. Figures 13(a-c) illustrate the change of the real part of complex modulus versus applied angular frequency for pure and L-Arginine (1 mol% and 2 mol%) doped KDP crystals at various temperatures. These figures show that at lower frequencies, the M' is nearly zero, indicating that there is no electrode-crystal polarization active in that frequency range. As the frequency increases, M' also increases, implying dispersive behaviour.

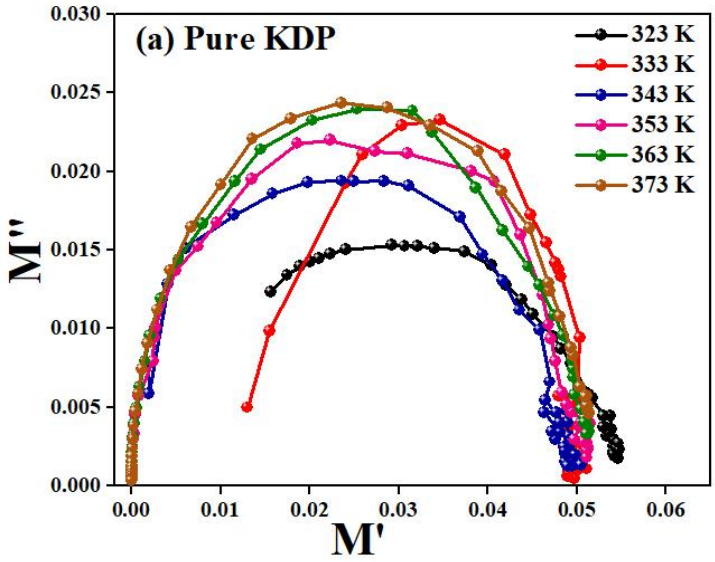

Figure 12(a). Variation in real (M') and imaginary (M'') parts of complex modulus for pure KDP crystal

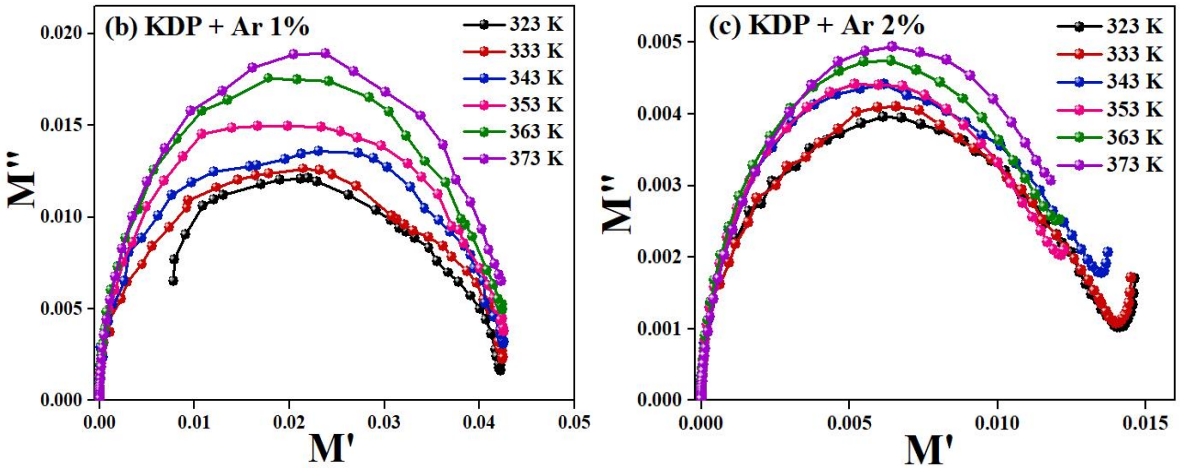

Figures 12. (b) Variation in real (M') and imaginary (M'') parts of complex modulus for L-Arginine (1 mol%) doped KDP crystal and **(c)** Variation in real (M') and imaginary (M'') parts of complex modulus L-Arginine (2 mol%) doped KDP crystal

Thus, charge carriers can flow along a long path at low frequencies under the influence of an applied electric field. Still, due to the lack of strong enough restoring force in this range, the value of M' is much lower for the temperature range under consideration [36]. The plots of the imaginary part of complex modulus (M'') versus applied angular frequency for pure KDP and L-Arginine (1 mol% and 2 mol%) doped KDP crystals are shown in Figures 14 (a-c). Each crystal has a single wide, asymmetric peak that corresponds to the grain effect within the crystals. As the temperature increases, the peaks shift to the higher frequency side due to ionic conductor behaviour [37], the peak frequency at which (M'') becomes maximum, known as the relaxation frequency.

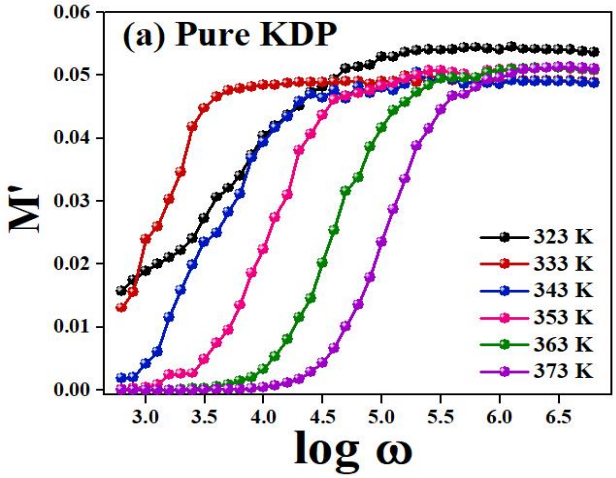

Figure 13(a). Variation of the real part of complex modulus (M') with angular frequency for pure KDP crystal

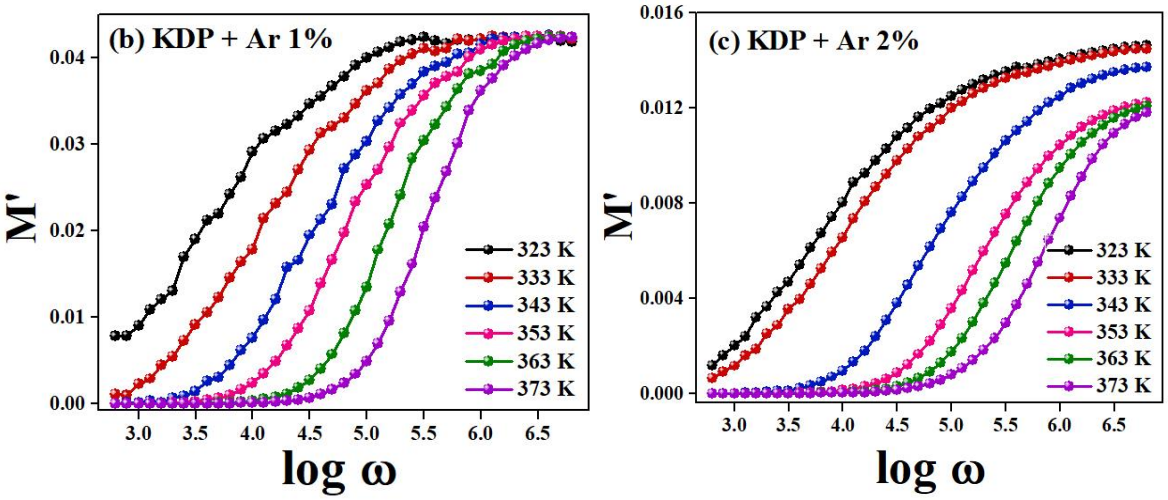

Figures 13. (b) Variation of the real part of complex modulus (M') with angular frequency for L-Arginine (1 mol%) KDP crystal and **(c)** Variation of the real part of complex modulus (M') with angular frequency for L-Arginine (2 mol%) KDP crystal

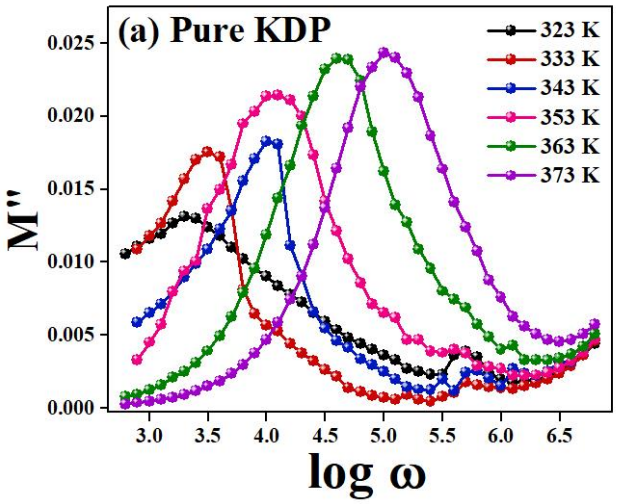

Figure 14(a). Variation of the imaginary part of complex modulus with angular frequency for pure KDP crystal

The stretch exponent parameter (β) can be used to validate the relaxation process in pure and doped KDP crystals. It is calculated using the following relation [38]:

$$\beta = \frac{1.196}{FWHM} - 0.047 \qquad (14)$$

where, FWHM is Full-Width Half Maximum of M'' versus *log ω* curve, obtained from curve fitting (Gaussian type).

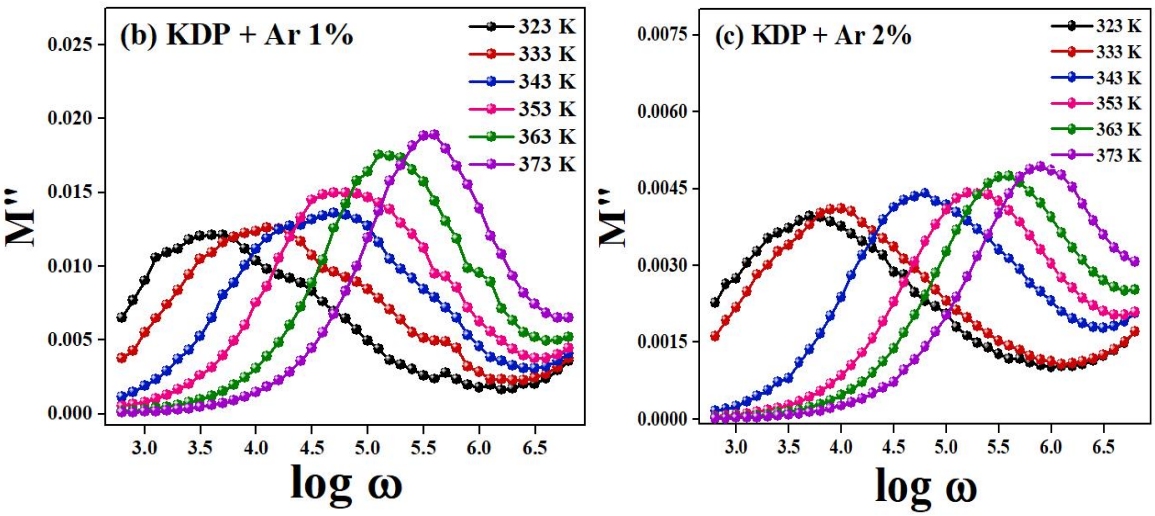

Figures 14. (b) Variation of the imaginary part of complex modulus with angular frequency for L-Arginine (1 mol%) doped KDP crystal and **(c)** Variation of the imaginary part of complex modulus with angular frequency for L-Arginine (2 mol%) doped KDP crystal

There are two case possibilities for β parameter: **(1)** If it is a non-Debye relaxation, the values β will fall between 0 to 1 depicting dipole-dipole interaction, and **(2)** If it is Debye type relaxation, the value of β will be unity which means there will be negligible dipole-dipole interaction, and it will be ideal dielectric relaxation. Here, for all the crystals studied, one relaxation peak is obtained for each temperature. Hence, the β-parameter for the grain relaxation was calculated separately, and the values obtained are summarized in table 7. It is seen that the stretch exponent parameter (β) deviates from unity for all crystals, indicating the presence of a non-Debye type relaxation mechanism in pure and L-Arginine doped KDP crystals.

Table 7. The calculated values of stretch exponent parameter (β) for pure KDP and L-Arginine (1 mol% and 2 mol%) crystals

Temperature	Stretch exponent parameter (β)		
	Pure KDP	KDP + Ar 1%	KDP + Ar 2%
323	0.5568	0.5768	0.6246
333	0.9104	0.5934	0.6813
343	0.9245	0.6159	0.7222
353	0.9363	0.6358	0.7710
363	0.9628	0.6901	0.5881
373	0.9237	0.7313	0.6347

3.3 Fourier Transform Infrared (FT-IR) Spectroscopy:

FTIR spectroscopy was used to investigate the effects of incorporating the amino acid L-Arginine with various functional groups on KDP. The spectra of pure and L-Arginine (1 mol% and 2 mol%) doped KDP crystals are shown in figure 15. The corresponding modes and functional groups of pure and doped KDP crystals are shown assigned in Table 8. Due to KDP bands overlapping amino acid vibrations, some frequencies are slightly shifted, and a few KDP bands tend to get broader. When comparing doped KDP crystals with pure KDP crystals, the absorption corresponding to NH stretching of NH^{3+}, C-N-H stretching of CH^2, and CH are present in doped KDP crystals, which shows that L-Arginine was successfully doped in KDP. The NH^{3+} stretching vibrations of amino acids emerge in the 2700-3300 cm^{-1} range, coinciding with the OH stretching vibrations of KDP. The unification of dopants in KDP is revealed by the functional groups of amino acids found in doped KDP crystals [39]. The spectra of L-Arginine doped KDP crystals indicate symmetric stretching of C–H, C= O, and COOH groups. Here, the dopant L-Arginine is expected to create L-defects by combining an unoccupied H-vacancy with the hydrogen atom of KDP. As a result of this, the basic vibration of hydrogen is rehabilitated.

Table 8. Functional groups of pure and L-Arginine (1 mol% and 2 mol%) doped KDP crystals

Bond Assignments	Wavenumber (cm^{-1})		
	Pure KDP	**KDP + Ar 1%**	**KDP + Ar 2%**
O-H vibration	3321	3325	3325
NH_3 asymmetric stretching	-	3398	3245-3397
N-H stretching	-	2921	2920
O-H asymmetric stretching	2927	2925	2921
O-P-OH symmetric stretching	1704	1678	1678
O-H bending	1630	1631	1631
O=P-OH stretch	1614-1695	1631	1631-1678
O=P-OH stretching	1652	1656	1657
NH_3 bending	-	1453	1452
P-O-H bending	1448	1453	1452
C-COO^- symmetric stretching	-	1416	1416
C-N-H stretching	-	1302	1300
P=O stretching	1295	1098	1099
P-O-H stretching	909	910	911
NO_3 stretching	-	774	774
COOH rocking	-	676	669
COO^- bending	-	617-669	617-669
HO-P-OH bending	533	536	536
NH_2 bending	-	534	534

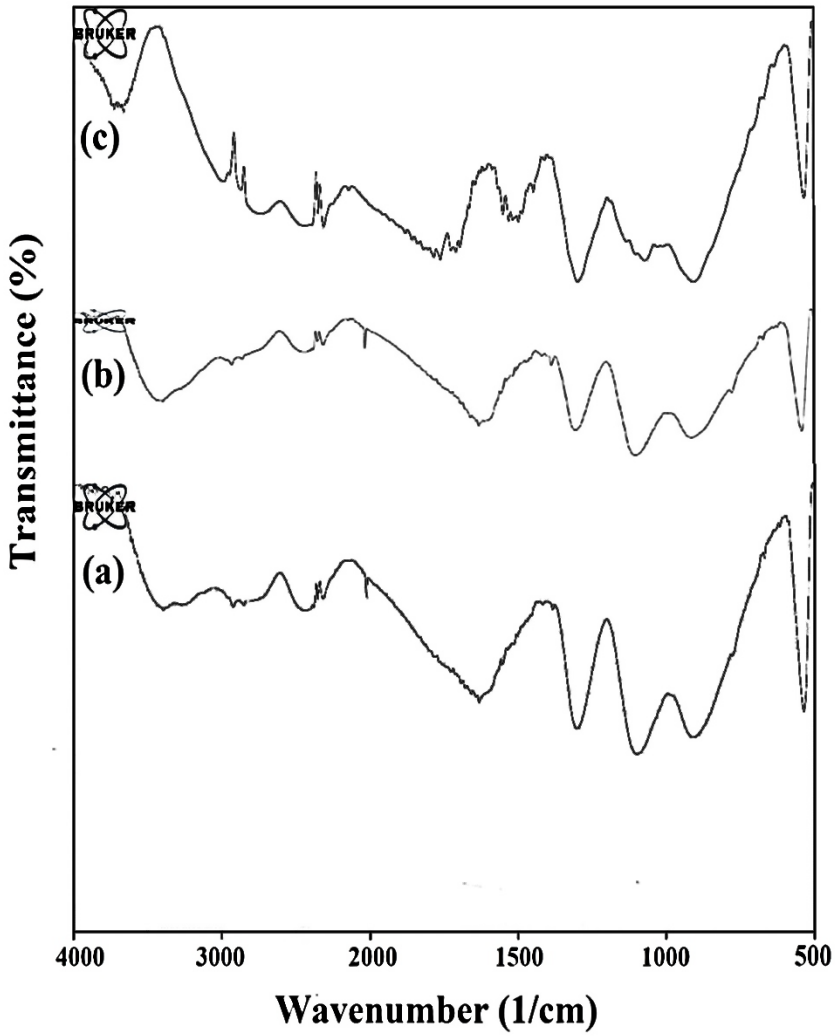

Figure 15. (a) FTIR spectrum of pure KDP crystal, **(b)** FTIR spectrum of L-Arginine (1 mol%) doped KDP crystal and **(c)** FTIR spectrum of L-Arginine (2 mol%) doped KDP crystal

Using the equation below, correlating absorption frequency and force constant, we determined the force constant of O–H vibration [40]:

$$\upsilon = 1330\sqrt{F\left(\frac{1}{M_1}+\frac{1}{M_2}\right)} \tag{15}$$

where, F is the force constant ($N.m^{-1}$), υ is the Absorption frequency (cm^{-1}), $1330 = (N_A \times 10)^{1/2}/2\pi C$, N_A= Avogadro number and M_1 and M_2 are the Molecular masses of molecules. Table 9 shows the calculated values of the force constant of O-H vibrations. As a result of the inclusion of L-Arginine into the KPD lattice, the values of force constant are reformed.

Table 9. The calculated values of Force Constant of O-H vibration of pure and L-Arginine doped KDP crystal

Sample	Absorption Wavenumber (cm^{-1})	Force Constant (Nm^{-1})
Pure KDP	3321	591.14
KDP + Ar 1%	3398	618.86
KDP + Ar 2%	3397	618.50

3.4 Ultraviolet-Visible (UV-Vis) Spectroscopy:

The absorbance spectra of pure and L-Arginine (1 mol% and 2 mol%) doped KDP crystals are shown in figure 16(a). In the visible region, the spectra indicate a high level of transparency. With increasing L-Arginine doping concentration in KDP, the optical transmittance increases uniformly. Using the following expression, the absorption coefficient (α) was determined from the absorbance data:

$$\alpha = \frac{2.303\ log_{10}\left(\frac{1}{T}\right)}{d} \tag{16}$$

where, T is the transmittance and d is the thickness of the crystal.

The optical energy bandgap (E_g) was calculated using the following equation from the transmittance and optical absorption coefficient α near the absorption edge.

$$\alpha hv = A\left(hv - E_g\right)^2 \tag{17}$$

where, v is the frequency, h is Planck's constant, A is constant, and E_g is the Optical bandgap.

The Tauc's plot is used to calculate the optical energy bandgap (E_g) of pure and L-Arginine (1 mol% and 2 mol%) doped KDP crystals by extrapolating the straight-line region of the plot on the X-axis, as illustrated in figures 16(b-c).

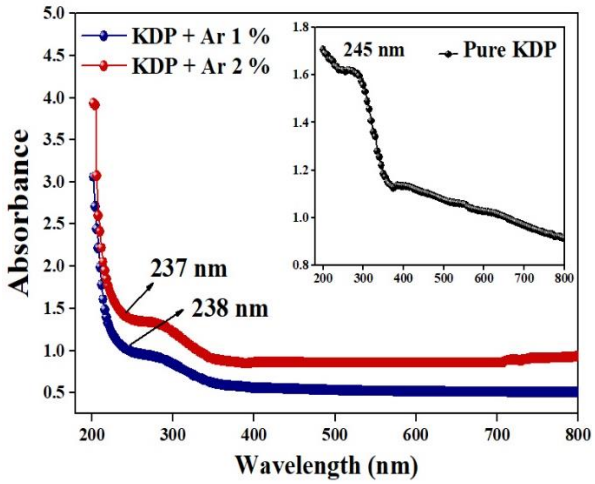

Figure 16(a). Absorbance spectra for pure and L-Arginine (1 mol% and 2 mol%) doped KDP crystals

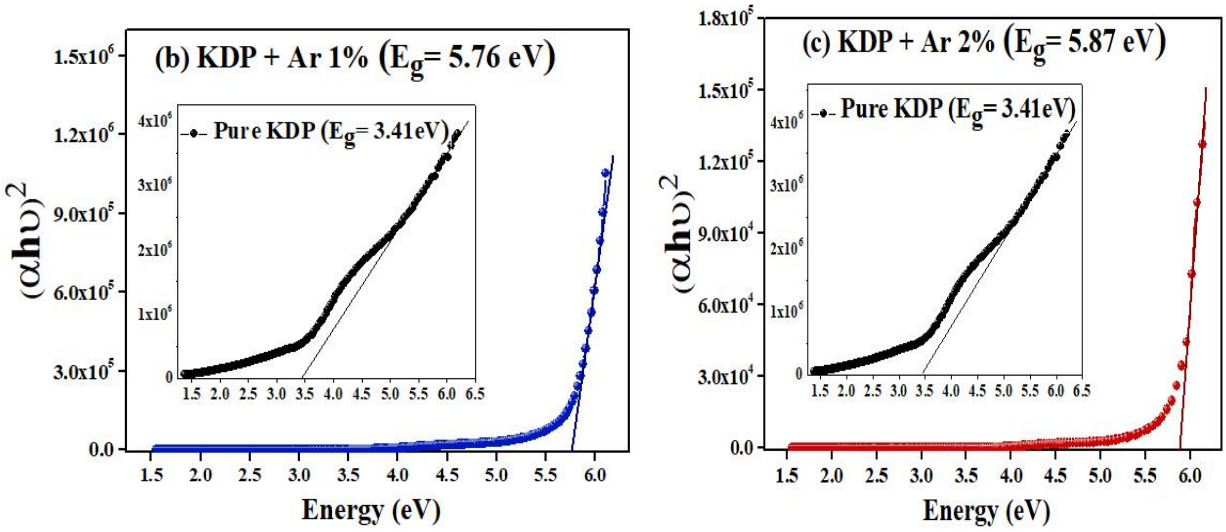

Figures 16. (b) Tauc's plot of L-Arginine (1 mol%) doped KDP crystal and **(c)** Tauc's plot of L-Arginine (2 mol%) doped KDP crystal

The optical band gaps of pure KDP, L-Arginine (1 mol%) doped KDP and L-Arginine (2 mol%) doped KDP crystals are 3.41 eV, 5.76 eV and 5.87 eV. It is observed that L-Arginine doped KDP crystals have large bandgap values, which makes them suitable for optoelectronic device fabrication [41]. The crystals with a large bandgap are required for nonlinear optical applications because the energy bandgap of the crystal demonstrates the ability of the dielectric medium (crystal) to be polarized under the effect of intense radiation. The following equation is used to compute the refractive index of pure and L-Arginine doped KDP crystals [42].

$$\eta = \frac{1}{T} + \sqrt{\frac{1}{T} - 1} \tag{18}$$

where, η is the refractive index and T is the transmittance.

The variation of refractive index with wavelength for pure and L-Arginine (1 mol% and 2 mol%) doped KDP crystals is shown in figure 17. As the wavelength increases, the refractive index of all the samples decreases. Such crystals can be good candidates for antireflection applications.

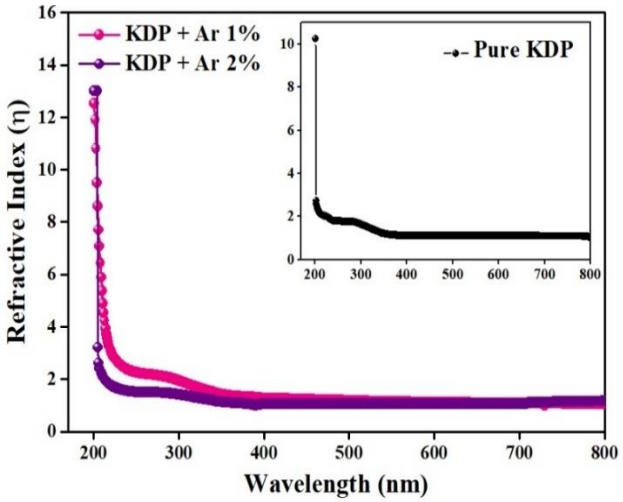

Figure 17. Variation of refractive index with wavelength for pure and L-Arginine (1 mol% and 2 mol%) doped KDP crystals

The ordinary and extraordinary refractive indices of KDP are computed using the following expression [43]:

$$\eta_o = 2.25881 + \frac{11.86370\,\lambda^2}{\lambda^2-400} + \frac{0.01041}{\lambda^2-0.01209} \tag{19}$$

$$\eta_e = 2.13338 + \frac{2.93795\,\lambda^2}{\lambda^2-400} + \frac{0.00873}{\lambda^2-0.01203} \tag{20}$$

where, η_o is the ordinary refractive index and η_e is the extraordinary refractive index and λ is the wavelength.

The calculated values of the η_o and η_e for KDP are found to be 1.5128 and 1.4656, respectively. Here, $\eta_o > \eta_e$ which correlates to the negative uniaxial aspect of the KDP crystal and can be used in birefringence applications. The extinction coefficient measures how much light is lost per unit distance of the participating medium due to scattering and absorption. The extinction coefficient can be calculated using the following relation:

$$K = \frac{\lambda\alpha}{4\pi} \tag{21}$$

where, α is the absorption coefficient and λ is the wavelength.

The variation in extinction coefficient K as a function of photon energy (hv) for pure and L-Arginine (1 mol% and 2 mol%) doped KDP crystals is shown in figure 18. The extinction coefficient of all crystals increases as photon energy increases. This could be due to scattering and absorption behaviour differences based on photon energy and scattering centre type. When compared to pure KDP crystal, the magnitude of the extinction coefficient for L-Arginine (1 mol% and 2 mol%) doped crystal is slightly higher. This result agrees with the refractive index and transmittance measurements.

The amount of electromagnetic radiation that penetrates a substance is measured by the skin depth (δ). It is defined as:

$$\delta = \frac{1}{\alpha} \tag{22}$$

where, δ is the Skin Depth and α is the Absorption coefficient.

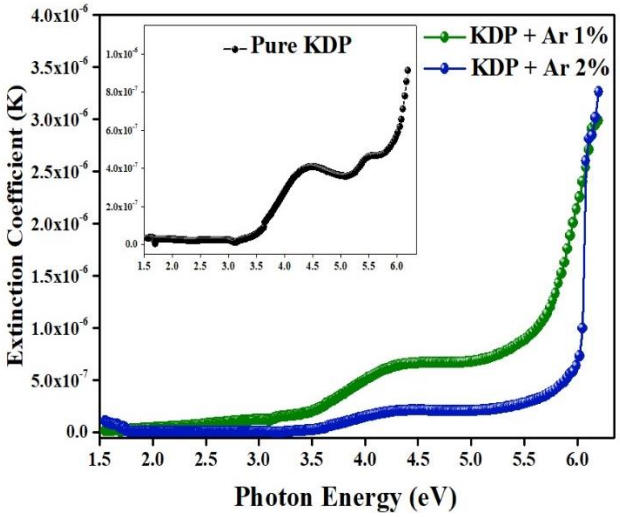

Figure 18. Extinction Coefficient of pure and L-Arginine (1 mol% and 2 mol%) doped KDP crystals

The variation of skin depth (δ) with photon energy (eV) for pure and L-Arginine (1 mol% and 2 mol%) doped KDP crystals is shown in figure 19. A sudden increase of skin depth was observed in the low photon energy range with a sharp peak. In addition, when the doping concentration of L-Arginine in KDP increases, the peak shifts into the higher photon energy region. However, the magnitude of the skin depth decreases with the concentration of L-Arginine in KDP crystal.

The optical conductivity is a measurement of its frequency response when a substance is irradiated with light. It is given as [44,45],

$$\sigma_{o.p} = \frac{\alpha \eta c}{4\pi} \tag{23}$$

where, c is the speed of light (vacuum), η is the refractive index and α is the absorption coefficient.

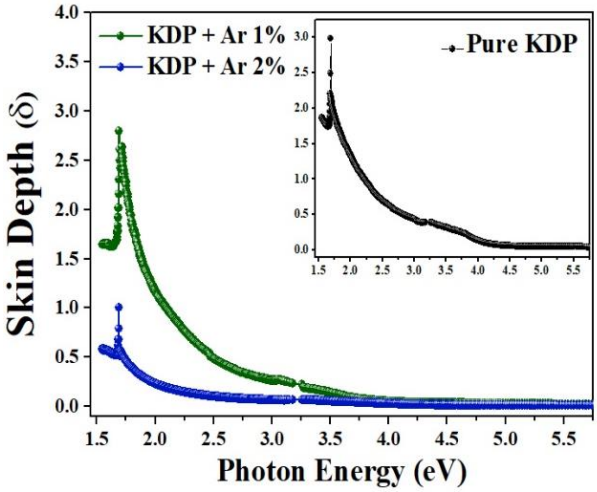

Figure 19. Variation of Skin depth (δ) w. r. t photon energy for pure and L-Arginine (1 mol% and 2 mol%) doped KDP crystals

Figure 20 shows the variation of optical conductivity with photon energy for pure and L-Arginine doped KDP crystals. It is observed that with an increase in photon energy, the optical conductivity also increases. Also, with doping concentration, the optical conductivity increases, which suggests that the higher the optical conductivity, the higher the conversion efficiency of the crystal.

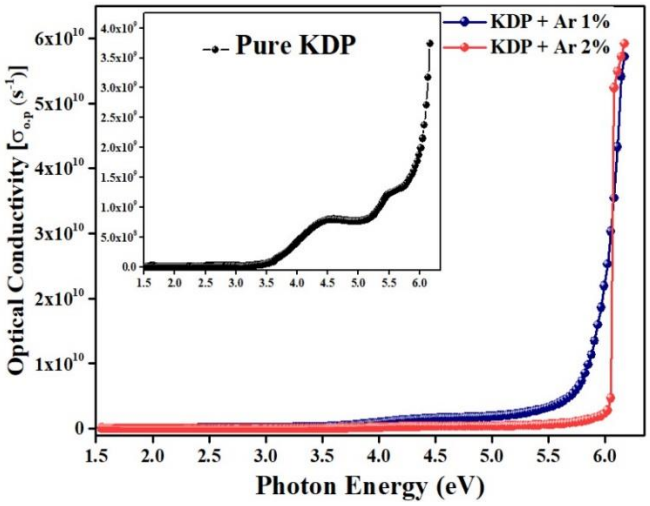

Figure 20. Optical Conductivity of pure and L-Arginine (1 mol% and 2 mol%) doped KDP crystals

3.4.1 Wemple-DiDomenico Single Oscillator Model Analysis:

Wemple and DiDomenico proposed a single oscillator model [46] in 1971 for the interband transition of electrons in the Brillouin zone that acts as an individual oscillator and identifies the valence electrons of atoms contributing to one such oscillator. This model is useful for investigating the dependence of the refractive index below the bandgap energy region (interband absorption edge) for nonlinear optical applications. This dependence of refractive index on photon energy below interband absorption edge is given as,

$$\eta = 1 + \frac{E_o E_d}{(E_o^2 - E^2)} \tag{24}$$

where, η is the refractive index, E_d is the dispersion energy, E_o is the single oscillator energy, and E is the photon energy.

Figure 21 represents the refractive index dispersion with photon energy below the absorption edges of pure and L-Arginine doped KDP crystals. The intercept and slope of the plot mentioned above were determined using linear fitting. The following equations were used to determine the values of E_o and E_d:

$$E_o = \sqrt{\frac{Intercept}{slope}} \quad \text{and} \quad E_d = \frac{E_o}{Intercept} \tag{25}$$

Table 10 shows the calculated values of E_o and E_d. It is observed that the value for the single oscillator increases with the increase in L-Arginine concentration; however, a reverse trend is observed in the case of dispersion energy. The average bond strength of any material is related to its single oscillator energy (E_o) which is known as cohesive energy. It is the difference in the average energy of free atoms and atoms of the crystal. Furthermore, the L-Arginine (2 mol%) doped KDP crystals have the highest dispersion energy compared to the other concentrations, favouring the incorporation of L-Arginine to a greater extent. Thus, crystals with this concentration may have superior nonlinear optical properties.

Table 10. Dispersive parameters of pure and L-Arginine (1 mol% and 2 mol%) doped KDP crystals

Sample	E_d (eV)	E_o (eV)
Pure KDP	3.88	6.15
KDP + Ar 1%	3.65	6.34
KDP + Ar 2%	3.20	6.46

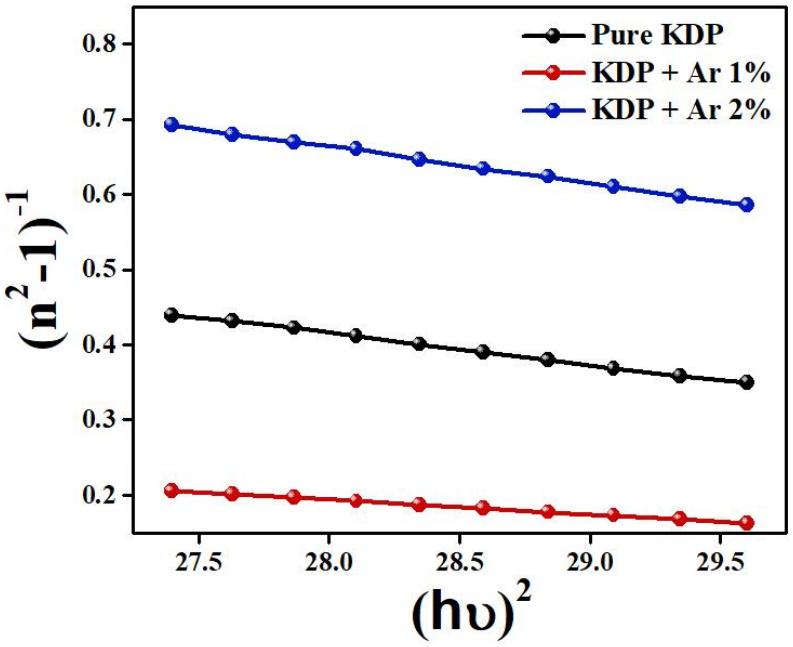

Figure 21. Wemple-DiDomenico model plots for pure and L-Arginine (1 mol% and 2 mol%) doped KDP crystal

3.4.2 Urbach Energy (Absorption band tail):

An inorganic substance's composition and optical bandgap can be determined using its optical absorption spectrum [47]. The optical absorption spectra of materials are divided into three regions: **(1)** Weak absorption region {presence of defects and impurities} **(2)** Absorption edge region {structural perturbation and disorder in the system} **(3)** Strong adsorption region {giving the optical bandgap energy}. The Urbach tail is the part of the absorption coefficient curve that is exponential at the optical band edge. The Urbach empirical rule describes the relationship between absorption coefficient (α) and photon energy at the optical bandgap edge and is provided by the equation:

$$\alpha = \alpha_o \exp\left(\frac{hv}{E_u}\right) \tag{26}$$

where, hv is the photon energy, E_u is the Urbach energy (exponential absorption edge width) and α_o is a constant.

The logarithm on both sides of equation (27) is used to obtain a straight-line equation as given below:

$$ln(\alpha) = ln(\alpha_o) + \frac{hv}{E_u} \tag{27}$$

The E_u value was calculated using the slopes of the straight-line plots shown in figure 22. $ln(\alpha)$ versus photon energy (eV) was plotted for obtaining the values of E_u. The calculated values of E_u are listed in table 11.

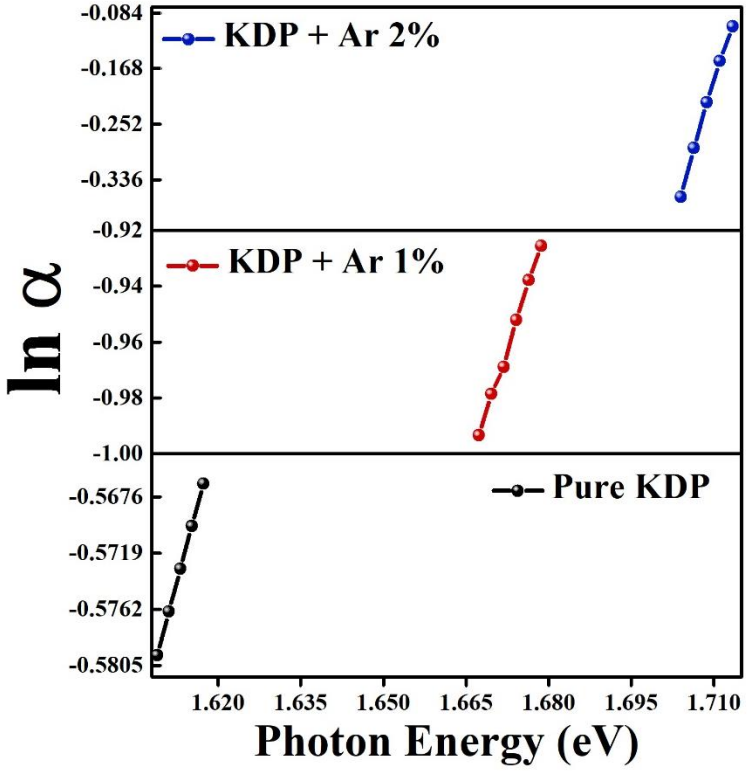

Figure 22. Urbach energy plot for pure and L-Arginine (1 mol% and 2 mol%) doped KDP crystal

With a rise in doping percentage, the Urbach energy of the L-Arginine (1 mol% and 2 mol%) doped KDP crystal decreases. The band tail expands as the disorder level increases because of the increased band to tail and tail to tail transitions. This condition is said to induce state redistribution and the formation of one-to-one tail states at the expense of band states [48].

Table 11. The calculated values of Urbach energy (E_u) for pure and L-Arginine (1 mol% and 2 mol%) doped KDP crystals

Sample	Urbach Energy (E_u) (eV)
Pure KDP	0.6391
KDP + Ar 1%	0.1651
KDP + Ar 2%	0.0364

3.5 Photoluminescence (PL) Analysis:

The photoluminescence emission spectra and excitation spectra of pure and L-Arginine (1 mol% and 2 mol%) doped KDP crystals are shown in figures 23(a-b). Photoluminescence analysis is useful in examining the quality of impurity amalgamation and the quality of the crystals. One of the optical processes that may be investigated using photoluminescence emission at a certain wavelength is the recombination of electronic transitions. The wavelength of PL excitation used was 247 nm. The crystal structure of pure KDP has various intrinsic lattice defects, the most basic of which are the unoccupied hydrogen vacancy (L-defect) and the double hydrogen bond (D-defect) [49]. As seen in table 12, the spectrum shows two emission peaks at different wavelengths. The centre, which is based on a hydrogen vacancy (L-defect) associated with a heterovalent impurity, is responsible for the excitation in the crystal's transparency region. Compared to pure KDP, the intensity of the PL emission spectra of L-Arginine (1 mol%) doped KDP is lower. This is because the dopant will destabilize the orientational L-defect in the vicinity of impurity atoms for charge compensation when the amino acid molecule is introduced in the KDP lattice matrix, implying that when the amino acid molecule is introduced in the KDP lattice matrix, the dopant will destabilise the orientational L-defect in the vicinity of impurity atoms. The electric studies of pure and L-Arginine doped KDP confirm the assumptions mentioned above.

Furthermore, it is found that the dopant creates hydrogen vacancies in the lattice of KDP, resulting in higher conductivity than pure KDP. As seen in table 13, the Stokes shift increases as the doping concentration of L-Arginine is increased. This behaviour is because L-Arginine has two charges, NH^{3+} (positive) and COO- (negative), due to which a dipole is created, and the KDP lattice surrounds it. The dipole moment of L-Arginine changes when it reaches the excited state under the influence of electromagnetic radiation, but the KDP lattice cannot adjust to it quickly enough. As a result, when the system's vibrations relax, its dipole moments realign with the applied optical field. As a result, as the doping concentration of L-Arginine increases, it becomes more difficult for the KDP lattice to realign, resulting in an increase in Stokes shift in ascending order of doping.

Table 12. PL Emission peaks for pure and L-Arginine (1 mol% and 2 mol%) doped KDP crystals

Sample	Emission Wavelength (nm)	
Pure KDP	370.89	468.86
KDP + Ar 1%	369.45	468.71
KDP + Ar 2%	369.21	468.24

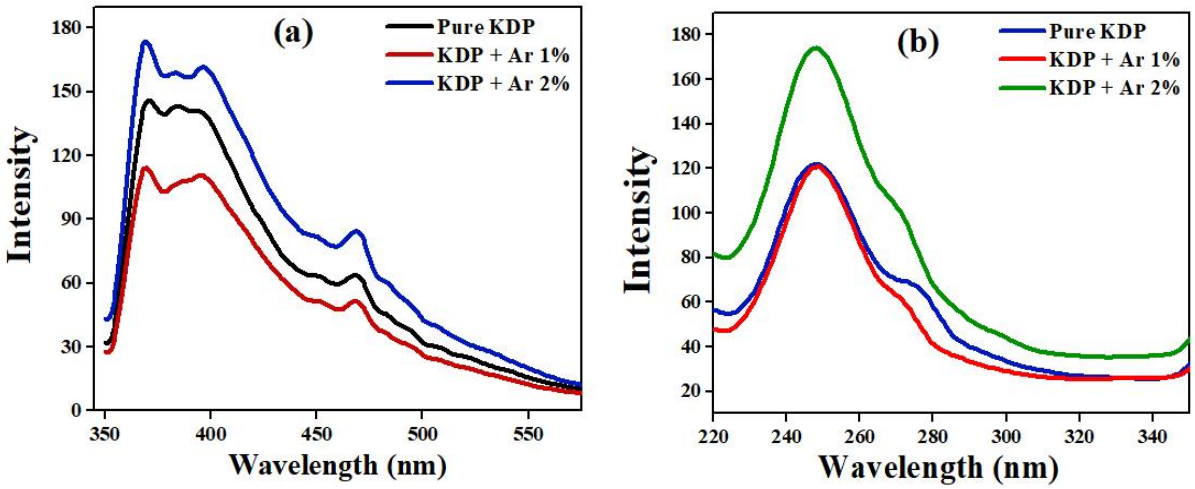

Figure 23. (a) PL Emission spectra of pure and L-Arginine (1 mol% and 2 mol%) doped KDP crystals and **(b)** PL Excitation spectra of pure and L-Arginine (1 mol% and 2 mol%) doped KDP crystals

Table 13. Variation in Stokes shift for pure and L-Arginine (1 mol% and 2 mol%) doped KDP crystals

Sample	Energy Absorption (eV)	Energy Emission (eV)	Stokes Shift (eV)
Pure KDP	4.9953	3.3446	1.6507
KDP + Ar 1%	4.9973	3.3576	1.6397
KDP + Ar 2%	5.0030	3.3598	1.6432

3.6 Relative Second Harmonic Generation (SHG) Efficiency:

The study of the NLO characteristics of KDP and L-Arginine doped KDP crystals reveals that the efficiency of SHG in doped KDP crystal samples is greater than in pure KDP crystals, as indicated in table 14. As the concentration of L-Arginine molecules increases, so does the intensity of radiation conversion. The efficiency of SHG increases proportionately with the increase in L-Arginine content in the crystal. The increased SHG efficiency of L-Arginine doped KDP crystals is attributed to NH^{3+} and COO^{-} groups in L-Arginine. These

optically active amino groups are responsible for the increase in non-centro symmetry, due to which the SHG efficiency increases. From the table, it may be possible that L-Arginine has a catalytic effect on the NLO properties of KDP. The increase in SHG efficiency is also likely attributable to the entry of the molecules and the formation of extra hydrogen bonds between the molecules and the crystal's growing face. Achieving second-order effects requires a favourable alignment of the molecule inside the crystal structure [50], which appears to be aided by doping. It has also been observed that changing the molecular orientation by inclusion complexation can substantially improve the SHG [51].

Table 14. Relative SHG efficiency of pure and L-Arginine (1 mol% and 2 mol%) doped KDP crystals

Sample	Relative SHG Efficiency
Pure KDP	-
KDP + Ar 1%	3
KDP + Ar 2%	2

4. Conclusion:

The pure and L-Arginine (1 mol% and 2 mol%) doped KDP crystals were successfully grown at room temperature with a slow evaporation technique. The obtained crystals were highly transparent. Powder XRD analysis revealed crystalline perfection and no substantial peak shifting, suggesting that the dopant L-Arginine atoms/molecules are accommodated adequately in the KDP crystal structure. The dielectric constant and dielectric loss decrease with applied angular frequency for all crystals due to electric dipole's inability to comply with the applied field and lattice defects produced within crystals. The a. c conductivity of doped KDP crystals is observed to be enhanced compared to pure KDP crystals suggesting the generation of defects in the lattice. From Jonscher's plots, we observed that L-Arginine doped KDP crystals follow the Correlation Barrier Hopping (CBH) conduction mechanism. Based on the conduction process taking place, we calculated the values of binding energy (W_m) and density of state at Fermi level [$N(E_f)$]. The incorporation of L-Arginine in the KDP lattice is confirmed by amino acid functional groups in the doped KDP spectra. Minor structural changes in the KDP crystalline matrix are caused by L-Arginine doping, evidenced by small shifts in vibrational frequencies in doped KDP crystal's FT-IR spectra. The bandgaps of L-Arginine (1 mol% and 2 mol%) doped KDP crystals are greater than those of pure KDP crystals. These findings suggest that the materials are suitable for the manufacture of optical devices. Doping

KDP crystal with L-Arginine (1 mol% and 2 mol%) successfully changed the transmittance cut-off, extinction coefficient, and refractive index in the visible area, critical for UV-tunable lasers, holographic data storage, and photonic devices. The huge magnitude of optical conductivity (10^{10} s^{-1}) confirms the presence of a very high photo responsive nature of the material. Crystals with low Urbach energy (E_u) values have a high degree of crystalline perfection. The PL emission spectra of pure and doped KDP crystals show that L- and D-defects exist in doped and pure crystals. In the PL emission spectra, electron and hole recombination at various photon energies has been observed. The Nd: YAG laser was used to examine the NLO properties of pure and doped crystals. The SHG efficiency of L-Arginine doped KDP (1 mol%) crystal was 3 times that of pure KDP, suggesting that it might be used in frequency conversions and other applications.

References:

1. Seethalakshmi. K, "*Growth and characterization of semi-organic L-Alanine family of single crystals"*, Manonmaniam Sundaranar University, Tamilnadu (2014).
2. A. K. Ghatak and K. Thyagarajan, *"Optical Electronics"*, Cambridge Uni. Press, Cambridge (1989) pp. 462-492.
3. N. Zaitseva, L. Carman, *J. of Prog. In Cryst. Growth and Charact.,* **43**(1) (2001) pp. 1-1118.
4. D. J. Williams, *"Nonlinear Optical Properties of Organic and Polymeric Materials, in: Proceedings of the American Chemical Symposium series"*, **233**, American Chemical Society, Washington, DC (1993).
5. H. J. Kolb and J. J. Comer, *J. American Chem. Soc.*, **67** (1945) pp. 894-897.
6. G. G. Muley, M. N. Rode, B. H. Pawar, *Acta Phys. Pol. A*, **116** (2009) pp. 1033-1038.
7. G. Deepa, T. H. Freeda, C. Mahadevan, *Indian J. Phys.,* **76 (A)** (2002) 369.
8. C. Razetti, M. Ardoino, L. Zanotti, M. Zha and C. Paorici, *Crys. Res. Technol.*, **37** (2002) pp. 456-465.
9. S. B. Monaco, L. E. Davis, S. P. Velsko, F. T. Wang, and D. Eimerl, *J. Crystal Growth*, **8** (1987) pp. 252-255.
10. H. O. Marcy, M. J. Rosker, L. F. Warren, P. H. Cunningham, C. A. Thomas, L. A. Deloach, S. P. Velsko, L. A. Ebbers, J. H. Liao, and M. G. Kanatzidis, *Opt. Lett.,* **20** (1995) pp. 252-254.
11. M. D. Agarwal, J. Choi, W. S. Wang, K. Bhat, R. B. Lal, A. D. Shields, B. G. Penn, and D. O. Frazier, *J. Cryst. Growth*, **204** (1999) pp. 179-182.
12. M. S. Pandian, K. Boopathi, P. Ramasamy, G. Bhagavannarayana, *Mater. Res. Bull.*, **47** (2012) pp. 826-835.
13. D. Xue, K. Kitamura, *Sol. Sta. Commu.*, **122** (2002) pp. 537-541.
14. K. S. Udapa, P. M. Rao, S. Aithal, A. P. Bhat, D. K. Avasthi, *Bull. Mater. Sci.*, **20** (1997) pp. 1069-1077.
15. M. Shakir, B. K. Singh, R. K. Gaur, B. Kumar, G. Bhagavannarayana, M. A. Wahab, *Chalcogenide Lett.*, **6**(12) (2009) pp. 655-660.
16. T. G. Reddy, B. R. Kumar, T. S. Rao, J. A. Ahamad, *Int. J. Appl. Eng. Res.*, **6**(5) (2011) pp. 571-580.
17. P. Jaita, A. Watcharapasorn, N. Kumar, D. P. Cann, S. Jiansirisomboon, *Elect. Mater. Lett.*, **11**(5) (2015) pp. 828-835.

18. T. Kanagasekaran, P. Mythili, B. Kumar, R. Gopalakrishnan, *Nucl. Inst. Met. Phy. Res.*, **268**(1) (2010) pp. 36-41.

19. B. T. Hatton, K. Landskron, W. J. Hunks, M. R. Bernett, D. Shukaris, D. D. Perovic, G. A. Ozinaa, *Mater. Today*, **9**(3) (2006) pp. 22-31.

20. E. J. Abram, D. C. Sinclair, A. R. West, *J. Electroceramics*, **10** (2003) pp. 165-177.

21. J. C. Dyre, *J. Non-Crystalline Solids*, **88**(2-3) (1986) pp. 271-280.

22. H. Fjeld, D. M. Kepaptsoglou, R. Haugsrud, T. Norby, *Solid State Ionics*, **181**(3-4) (2010) pp. 104-109.

23. M. M. Costa, G. F. M. Pires, A. J. Terrozo, M. P. F. Graca, A. S. B. Somba, *J. Appl. Phys.*, **110** (2011) pp. 034107(1-7).

24. K. K. Bharathi, G. Marukandeyulu, C. V. Ramana, *J. Electrochem. Soc.*, **158**(3) (2011) G71-G78.

25. K. Hayat, *Phys. B*, **406**(3) (2011) pp. 309-314.

26. M. Ben Bechir, K. Karoui, M. Tabellout, K. Guidara, A. Ben Rhaiem, *J. Appl. Phys.*, **115** (2014) pp. 153708(1-8)

27. N. V. Prasad, K. Srinivas, A. R. James, *Ferroelectrics*, **282**(1) (2003) pp. 217-228.

28. K. Funke, *Prog. Sol. Sta. Chem.*, **22**(2) (1993) pp. 111-195.

29. J. P. Tiwari, K. Shahi, *Philosophical Magazine*, **87**(29) (2007) pp. 4475-4500.

30. S. Mollah, K. K. Som, B. K. Bose, J. Chaudhuri, *J. Appl. Phys.*, **74** (1993) pp. 931-937.

31. S. R. Lukic-Petrovic, F. Skuban, D. M. Petrovic, M. Slankamenac, *J. Non-Crystalline Solids*, **356**(44-49) (2010) pp. 2409-2413.

32. K. Prasad, K. Kumari, K. P. Chandra, K. L. Yadav, S. Sen, *Mater. Sci. Poland*, **27**(2) (2009) pp. 373-384.

33. A. Kahouli, A. Sylvestre, F. Jomni, B. Yangui, J. Legrand, *J. Phys. Chem. A.*, **116**(3) (2012) pp. 1051-1058.

34. F. Yakuphanoglu, Y. Aydogdu, U. Rentscheter, *Sol. Stat. Commu.*, **128**(2-3) (2003) pp. 63-67.

35. M. A. Afifi, A. E. Berkheet, E. Elwahabb, H. E. Atvia, *Vacuum*, **61**(1) (2001) pp. 9-17.

36. P. B. Macedo, C. T. Maynihan, R. Bose, *Phys. Chem. Glasses*, **13** (1972) pp. 171-179.

37. A. Ben Rhaiem, F. Hlel, K. Guidara, M. Gargouri, *J. Alloy. Compd.*, **463**(1-2) (2008) pp. 440-445.

38. P. K. Dixson, *Phys. Rev. B*, **42** (1990) pp. 8179-8186.

39. A. Mahadik, P.H. Soni, K. Chaudhari, *AIP Conference Proceedings*, **2265** (2020) pp. 030421(1)-030421(4).

40. N. B. Colthup, L. H. Dal, S. E. Wiberley, *"Introduction to Infrared and Raman Spectroscopy"*, Academic Press, London (1975).

41. M. Parthasarathy, M. Anantharaja, R. Gopalakrishnan, *J. Cryst. Growth*, **340**(1) (2012) pp. 118-122.

42. N. A. Bakr, A. M. Funde, V. S. Waman, M. M. Kamble, R. R. Hawaldar, D. P. Amalnerkar, S. W. Gosavi, S. R. Jadkar, *Pramana*, **76** (2011) pp. 519-531.

43. Lili Zhu, Xiang Zhang, Mingxia Xu, Baoan Liu, Shaohua Ji, Lisong Zhang, Hailiang Zhou, Fafu Liu, Zhengping Wang and Xun Sun, *AIP Advances*, **3** (2013) pp. 112114(1-8).

44. P. A. Ilenikhena, *African Phys. Rev.*, **2** (2008) pp. 68-77.

45. J. I. Pankove, *"Optical Processes in Semiconductors"*, Prentice Hall, New York (1971).

46. S. H. Wemple and M. DiDomenico, *Jr. Phys. Rev. B*, **3**(4) (1971) pp. 1338-1350.

47. A. S. Hassanien, and Alaa A. Akl, *Superlattice Microst.*, **89** (2016) pp. 153-169.

48. K. Stephen et al., *J. Non-Cryst. Solids*, **210** (1997) pp. 249-253.

49. Mohd. Hasmuddin, P. Singh, Mohd. Shkir, M. M. Abdullah, N. Vijayan, V. Ganesh, M. A. Wahab, *J. Mater. Chem. and Phys.*, **144** (3) (2014) pp. 293-300.

50. S. R. Hall, P. V. Kolinsky, R. Jones, S. Allen, P. Gordon, B. Bothwell, D. Bloor, P. A. Norman, M. Hursthouse, A. Karaulov, J. Baldwin, M. Goodyear, D. Bishop, *J. Cryst. Growth*, **79**(1-3) (1986) pp.745-751.

51. Y. Wang D. F. Eaton, *Chem. Phys. Lett.*, **120**(4-5) (1985) pp. 441-444.